Investigation of Non-contact Bearing Systems Based on Ultrasonic Levitation

zur Erlangung des akademischen Grades eines

DOKTORS DER INGENIEURWISSENSCHAFTEN (Dr.-Ing.)

der Fakultät für Maschinenbau

der Universität Paderborn

genehmigte

DISSERTATION

von

M. Sc. Su Zhao

aus *Liaoning, VR China*

Tag des Kolloquiums: 19.03.2010

Referent: Prof. Dr.-Ing. Jörg Wallaschek

Korreferent: Prof. Dr.-Ing. habil. Ansgar Trächtler

Abstract

Non-contact bearings based on acoustic/ultrasonic levitation are investigated in this thesis. Both standing wave type and squeeze film type ultrasonic levitation are investigated theoretically and experimentally.

The conventional standing wave type ultrasonic levitation has not found technical applications in non-contact bearings due to the fact that it has very limited load capacity and can only levitate elements which are smaller than the sound wavelength. In this thesis work, a new configuration of standing wave levitation is presented which is able to levitate large planar object at a position of multiple times of a half wavelength of the sound wave. The theoretical model for the proposed levitation system is established and a prototype system is constructed accordingly. A CD is successfully levitated with the proposed system at a height of half a wavelength. A levitation force of 1 N is measured at the position of half wavelength.

Squeeze film type ultrasonic levitation is investigated theoretically to find the crucial design parameters and to improve the levitation capacity. Two analytical models based on acoustic theory and fluid dynamics are presented and compared. The governing fluid dynamics equation is solved numerically to obtain precise pressure distributions. Based on the theoretical investigation, a novel non-contact journal bearing is developed for suspension of a solid steel spindle with diameter of 50 mm. The maximum load capacity of 51 N (6.37 N/cm^2) is obtained which is considerably larger than the previously reported squeeze film bearings whose load capacities are usually within a few Newton (less than 1 N/cm^2).

Zusammenfassung

Im Rahmen dieser Arbeit werden berührungslose Lagerungen mit akustischer Ultraschall-Levitation entwickelt und vorgestellt. Dabei werden sowohl Stehwellen-, als auch Squeezefilmlevitation theoretisch und experimentell untersucht.

Bisher wurde die Ultraschall Levitation mit stehenden Wellen aufgrund der begrenzten Lastaufnahme und der auf die halbe Wellenlänge begrenzten Objektgröße nicht in technischen Anwendungen als Lagerung appliziert. In dieser Arbeit wird ein neuer Aufbau vorgestellt, mit dem große ebene Objekte im Abstand einiger halber Wellenlängen levitiert werden können. Neben theoretischen Betrachtungen wird ein Prototyp aufgebaut, an dem bei einem Abstand einer halben Wellenlänge eine Levitationskraft von 1N gemessen werden kann. Damit kann erfolgreich eine CD levitiert werden.

Zur Auslegung und Optimierung der Squeezefilmlevitation werden zwei analytische Modelle, die einerseits auf der Akustik und anderseits auf der Fluiddynamik beruhen, vorgestellt und verglichen. Das akustische und das numerisch ausgewertete fluiddynamische Modell werden anschließend mit Hilfe von Messungen validiert. Basierend auf den Simulationen wird ein neuartiges berührungsloses Lager für eine Welle mit einem Durchmesser von 50 mm entworfen. Mit dem neuartigen Aufbau kann eine maximale Last von 51N ($6{,}37$ N/cm^2) aufgenommen werden und damit eine wesentlich höhere Traglast als mit vorhergehenden Squeezefilmlagern, deren Last auf wenige Newton (weniger als 1 N/cm^2) beschränkt war, erreicht werden.

Acknowledgements

This thesis represents the conclusion of my research from 2006 to 2009. I joined the International Graduate School Dynamic Intelligent System (IGS) in Universität Paderborn in April 2006. After one year stay, I followed my supervisor to Leibniz Universität Hannover and continued my study in the Institute for Dynamics and Vibration Research. During all these years, I have received help from so many people, and to them I would like to express my gratitude. I offer my apologies in advance if I miss to mention anyone who has help me. Also, after struggling long enough with the accuracy of my English in this document, I reserve the right to use a more conversational tone in this section.

First of all, it would have not been possible for me to live and study in Germany without the fellowship from IGS of Universitär Paderborn. Here I would like to thank Prof. Steffen for recruiting me and to Dr. Arnold Hueck-Stiftung for the fellowship. I am also thankful to my supervisor Prof. Wallaschek for continuing supporting me after the 3-year IGS program.

On the faculty side, I'd first like to thank my thesis supervisor Prof. Wallaschek for offering me the possibility to work in a liberal environment and giving me the freedom to conduct my research in a independent way. I am also deeply thankful to my thesis committee, Prof. Sextor, Prof. Trächtler and Prof. Schmid, for taking their time reviewing my work.

On the non-faculty side, I would like to thank all my colleagues in MUD and IDS. They have made me feel really comfortable at work. In particular, I'd

Contents

1

Motivation

Non-contact suspension of objects (with rotational or linear motion) has significant advantages in many situations. Being non-contact, the systems can be operated at much higher speeds than using conventional mechanical bearings. Also, there will not be problems such as overheating and wear of the bearing components any more. Thus, high precision and high speed of motion can be achieved.

Classical non-contact bearings such as air bearings and magnetic bearings are already being used in several practical applications. However, a continuous supply of a large volume of clean air is required for the air bearings, which leads to high running cost. And, the requirement of an external pump excludes this type of bearing from certain applications. Magnetic bearings can not be used for magnetically sensitive configurations due to the strong magnetic flux. It is therefore of great interest to find other concepts for realizing non-contact suspension which can resolve these problems.

Acoustic/ultrasonic levitation has been found to be a promising alternative solution. It has drawn great attention in the last decades and shown good potentials to overcome some of the shortcomings of the existing non-contact suspension methods. Non-contact bearings based on acoustic/ultrasonic levitation use air as lubricant. They share the advantages of classic air bearings. However, in acoustic/ultrasonic levitation the load-carrying pressure is generated internally by means of high frequency mechanical vibrations. Therefore, external supply of pressurized air is not needed anymore. The bearing can be as compact as two conforming surfaces. These distinct characteristics

make it suitable for certain situations where air or magnet bearings are not applicable. In the current thesis, theoretical and experimental investigations on non-contact bearings based on acoustic/ultrasonic levitation are performed.

2

State of the art

2.1 Non-contact bearings

A bearing is a device that supports and guides one machine component with respect to others in such a way that prescribed relative motion can occur while the forces associated with machine operation are transmitted smoothly and efficiently. Bearings may be classified broadly according to the motions they allow and according to their principle of operation as well as by the directions of applied loads they can handle. Here we classify bearings by whether or not a direct mechanical contact exists between the bearing and the supported member. In this way, bearings are classified into to contact and non-contact bearings.

Contact bearings are the most common used bearings such as plain rubbing bearings, ball bearings, and roller bearings, in which the load is supported by means of direct physical contact. These bearings have been developed since centuries and have very wide range of applications. Due to mechanical contact between rigid bodies, these bearings often suffer from wear, heat generation, vibration and noise generation, especially in high speed operations.

In non-contact bearings, there is no direct physical contact between the bearing and the load. In consequence, these bearings have no wear, nearly no friction (except for fluid drag) and they can achieve higher accuracies. Fluid film bearings are the most popular non-contact bearings. They use a thin film of fluid (liquid or gas) to separate

the two surfaces. The load-carrying capacity is derived from the pressure within the lubricating film and can be generated by the motion of the machine elements (self-acting or hydrodynamic/aerodynamic bearings) or by external pressurization (hydrostatic, or air bearings) or squeeze motion (squeeze film acoustic bearing, the main focus of this research work), or by a combination of these actions. Besides fluid film bearings, magnetic bearings are another type of non-contact bearing. They support a load using magnetic levitation force. Therefore, no lubricant or medium is needed to perform the levitation.

Non-contact bearings are frequently used in high load, high speed or high precision applications where ordinary rolling element bearings have short life or high noise and vibration. In the following part of this section, some typical non-contact bearings will be introduced and their strength and weakness will be discussed.

- Hydrodynamic bearing

In hydrodynamic bearings, the bearing rotation sucks the fluid onto the inner surface of the bearing, forming a lubricating wedge under or around the shaft. They are suited for improving rotational accuracy and enhancing quietness and robustness. These bearings have excellent damping properties due to squeeze film damping. The fabrication of hydrodynamic bearings is simple compared to dry-rubbing bearings, which leads to low cost for production. Hydrodynamic bearings have been successfully applied in computer hard drive industry to replace the conventional ball bearings. Hydrodynamic bearings rely on bearing motion to maintain the load-carrying pressure. They may suffer on high friction and short life at low speeds or during starts and stops.

- Hydrostatic bearing

Hydrostatic bearings use a pressurized liquid film to support the load. They rely on an external pump to constantly supply the pressurized liquid in the bearing clearance to maintain the film. Hydrostatic bearings have excellent damping as well as very high stiffness. They are widely used for high precision and high speed machine tools such

as precision milling machine, precision manufacturing center. The design of a hydrostatic bearing is more complicated than that of a hydrodynamic bearing. It requires the precise adjustment of a number of parameters including pad geometry, restricted size, supply pressure, and journal bearing clearance to optimize performance.

- Aerodynamic bearing

Aerodynamic bearings are analogous to hydrodynamic bearings. One major difference is that the lubricant is gas (normally air) which is compressible. Air also has a much lower (more than 1000 times less) viscosity than even the thinnest oils. Therefore the viscosity induced friction force is much smaller. Aerodynamic bearings have very distinct advantages and disadvantages. They allow extremely high operating speed and can be operated in extremely low or high temperatures. The lubricant is ample, clean and does not contaminate the surfaces and the surroundings. However, similar to hydrodynamic bearings, the load capacity is dependent on the relative speed at which the surface moves and therefore at zero speed, the bearing supports no load. Aerodynamic bearings have much lower load capacity compared to hydrodynamic bearings with similar size. Another weakness is that they generally have poor stability that can produce destructive contact between rotational and stationary components.

- Aerostatic bearing

Aerostatic bearings (often referred as air bearing) are similar to hydrostatic bearings, and use a thin pressured gas film to carry the loads. They need an external pressure source to create the air film. This type of bearing shares many of the advantages of the aerodynamic bearing. In addition, it supports load at zero speed. There are two types of air supply mechanism in aerostatic bearings, orifice type and porous carbon/metal type. In orifice type, the air is fed through the orifices into the bearing clearance. As air escapes from the orifice it expands and so its pressure drops as it flows across the face of the bearing resulting in variances of pressure in the air gap. In porous carbon/metal type, the air pressure drops as it flows through the porous layer. Even pressure then bleeds from the entire bearing face resulting in a more uniform pressure in the air gap. Porous carbon/metal type aerostatic bearings have advantages. They are more damage

tolerant, have higher air film stiffness and are naturally stable.

Aerostatic bearings are employed in many high speed and high precision machines doing work inside a micrometer or in nanometer range. They are also suitable for industries such as food productions or pharmaceutical productions where oil lubrication is a problem.

- Electromagnetic bearing

An electromagnetic bearing positions and supports a moving shaft using magnetic forces without mechanical contact. Magnetic bearings allow the highest rotating speed among all kinds of bearings since they are non-contact and require no lubricant at all. They work in extreme conditions such as vacuum as well. With position feedback control system, an electromagnetic bearing can be operated as an active bearing system which offers dynamic stiffness and error compensation abilities by varying the amount of current in the coils of the magnet system.

Electromagnetic bearings are increasingly used in industrial machines such as compressors, turbines, pumps, motors and generators. Electromagnetic bearings are also used in high-precision instruments. Unfortunately, electromagnetic bearings have some severe disadvantages. Magnetic force is an attractive force. It decreases with greater, and increases with smaller gap. This makes a magnetic bearing unstable from its nature. A control system must be installed to maintain the stable suspension. Continuous power supply is needed for most electromagnetic bearings. Therefore, some kind of back-up bearing is typically needed in case of power or control system failure. The magnetic flux leakage during operation can affect the sensitive electronics around the bearings.

Beside the existing types of non-contact bearings, ultrasonic levitation has been found as an alternative way to realize non-contact suspension. The basic theory underlying the operating principle of ultrasonic levitation will be discussed in the following section.

2.2 Ultrasonic levitation

An acoustic wave can exert a force on objects immersed in the wave field. These forces are normally weak, but they can become quite large when using high frequency (ultrasonic) and high intensity waves. The forces can even be large enough to suspend substances against gravity force. This technique is called acoustic levitation. Since the sound waves used are often in the ultrasonic frequency range (higher than $20kHz$), it is more often called as ultrasonic levitation.

Ultrasonic levitation has been firstly used for levitating small particles by creating a standing wave field between a sound radiator and a reflector, namely standing wave ultrasonic levitation. Standing wave type ultrasonic levitators with various features were designed for applications in different scientific disciplines such as containerless material processing and space engineering (53). Another well-known type of ultrasonic levitation is squeeze film ultrasonic levitation. It happens when a flat surface is brought to a conformal radiation surface which vibrates in high frequency. In the following part of this section, both types of ultrasonic levitation will be reviewed in detail.

2.2.1 Standing wave type

Standing wave levitation phenomenon was first observed in Kundt's tube experiment (41) in 1866, that small dust particles moved towards the pressure nodes of the standing wave created in a horizontal Kundt's tube. A typical setup for standing wave levitation is shown in Fig. 2.1. As a result of multiple reflections between an ultrasonic radiator and a solid, flat or concave reflector, a standing wave with equally spaced nodes and anti-nodes of the sound pressure and velocity amplitude will be generated. Solid or liquid samples with effective diameters less than a wavelength can be levitated below the pressure nodes. The axial suspension of the sample is an effect of the sound radiation pressure of a standing wave. Combining with a Bernoulli vacuum component, the sound wave can locate the samples laterally as well (11).

The first detailed theoretical description of standing wave levitation was given by King (28) in 1934. King's work was extended by Hasegawa and Yosioka (19) to include
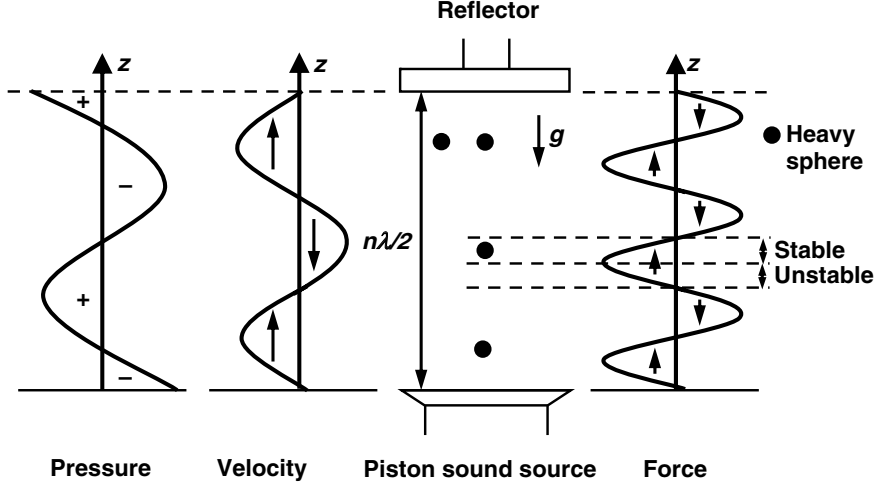
Figure 2.1: Distribution of sound pressure, air particles's velocity and levitation force in a standing wave type levitation system(53)

the effects of compressibility. Embleton (12) adopted King's approach to fit to the case of a rigid sphere in a progressive spherical or cylindrical wave field. Westervelt (57; 58; 59) derived a general expression for the force owing to radiation pressure acting on an object of arbitrary shape and normal boundary impedance. Westervelt showed that a boundary layer with a high internal loss can lead to forces that are several orders of magnitude greater than those predicted by the classical radiation pressure theory.

A very different approach compared to King was presented by Gor'kov (16), who presented a simple method to determine the forces acting on a particle in an arbitrary acoustic field. The velocity potential was represented as sum of an incident ϕ_{in} and a scattered term ϕ_{sc}. Barmatz (4) applied Gor'kov's method to derive the generalized potential and force expressions for arbitrary standing wave modes in rectangular cylindrical and spherical geometries. Lierke gave an overview of standing wave acoustic levitation (31) based on long term research and development activities for the European and the US space agencies. Xie and Wei (64) studied the acoustic levitation force on disk samples and the dynamics of large water drops in a planar standing wave, by solving the acoustic scattering problem through incorporating the boundary element method.

For understanding the basic working principles of standing wave levitation, the theoretical approach of King (28) will be discussed shortly in the following. Assuming that the fluid being considered is adiabatic and barotropic, the equations of motion can be written as:

$$\rho \frac{Du}{Dt} = -\frac{\partial p}{\partial x}, \quad \rho \frac{Dv}{Dt} = -\frac{\partial p}{\partial y}, \quad \rho \frac{Dw}{Dt} = -\frac{\partial p}{\partial z} \tag{2.1}$$

where

$$\frac{D}{Dt} = \frac{\partial}{\partial t} + u \frac{\partial}{\partial x} + v \frac{\partial}{\partial y} + w \frac{\partial}{\partial z}$$

is the absolute derivative, ρ the density of the medium, p the pressure, and (u, v, w) the Cartesian velocity components. By defining $\tilde{\omega} = dp/\rho$ the equation of motion can be rewritten as:

$$\frac{Du}{Dt} = -\frac{\partial \tilde{\omega}}{\partial x}, \quad \frac{Dv}{Dt} = -\frac{\partial \tilde{\omega}}{\partial y}, \quad \frac{Dw}{Dt} = -\frac{\partial \tilde{\omega}}{\partial z} \tag{2.2}$$

When the motion is irrotational, the velocity components can be expressed in terms of the velocity potential ϕ,

$$(u, v, w) = -\nabla \phi \tag{2.3}$$

In case of air as the medium, the velocity potential can be obtained from the approximate linear wave equation

$$\nabla^2 \phi = \frac{1}{c^2} \frac{\partial^2 \phi}{\partial t^2} \tag{2.4}$$

which is simplified from the exact differential equation for ϕ using a second order approximation. The equation of continuity is:

$$\frac{\partial \rho}{\partial t} + \frac{\partial}{\partial x} (\rho u) + \frac{\partial}{\partial y} (\rho v) + \frac{\partial}{\partial z} (\rho w) = 0 \tag{2.5}$$

and the pressure variation can then be derived from Eq. (2.5) as:

$$\Delta p = p - p_0 = p_0 \frac{\partial \phi}{\partial t} + \frac{1}{2} \frac{\rho_0}{c^2} \left(\frac{\partial \phi}{\partial t} \right)^2 - \frac{1}{2} \rho_0 q^2 \tag{2.6}$$

where ρ_0 is the density of the surrounding medium, ϕ is the velocity potential, c is the sound speed in air and q is the velocity amplitude equal to $\sqrt{u^2 + v^2 + w^2}$. Detail derivation of Equ. 2.6 can be found in Ref. (28). The time averaged acoustic pressure on a rigid body can be calculated by integrating the acoustic pressures acting on each surface element of the body.

2. STATE OF THE ART

In the case of a plane standing wave, the velocity potential ϕ_s can be expressed as (28):

$$\phi_s = |A| \cos kh \cos \omega t \tag{2.7}$$

where, $|A|$ is the amplitude of the velocity potential, $k = 2\pi/\lambda$ is the wave number, and h is the position where the sphere, which is assumed to be small, is located. The acoustic radiation force on a rigid sphere can be calculated as:

$$F = -\frac{5}{6}\pi\rho_0 |A|^2 (kR_s)^3 \sin(2kh) \tag{2.8}$$

with R_s being the radius of the sphere.

Bücks and Müller in 1933 (8) presented the first experimental setup for positioning of small samples in acoustic standing waves. A small particle was trapped at a position slightly below the pressure nodes of the standing wave between a radiator and a reflector. In 1974, Wang et. al. (55) presented an acoustic chamber for positioning of molten materials. The chamber was used for positioning in an extreme temperature gradient. In 1975, Whymark (60) proposed an acoustic levitator for positioning of materials in space using a single source of sound. Fine control of position could be obtained by adjusting the reflector. In 1983 Lierke (32) presented an acoustic levitator for positioning the materials samples in mirror furnaces in space processing. In 1985, Trinh (52) presented a compact acoustic levitation device for studies in fluid dynamics and materials science in microgravity. This classic structure was later modified to achieve better performances. Otsuka et. al. (40) used a stepped circular vibrating plate as the radiator which can produce high intensity ultrasound fields. Different from conventional piston-like vibration sources, this approach used the flexural vibration mode of the plate with two nodal rings to achieve higher vibration amplitude. The stepped plate has a concave channel with fixed depth of half sound wavelength in air. This special design makes the concave and convex blocks vibrate in the counter phase so that the ultrasound propagating in the air is modulated in the same phase. As a result, a narrow, intensive, high directional ultrasound beam is obtained. In 2001, Xie and Wei (63) enhanced the standing wave acoustic levitation force by properly curving the surface and enlarging the reflector. High density material like tungsten ($\rho = 18.92 g/cm^3$) was successfully levitated for the first time using standing wave ultrasonic levitation. Recently in 2006, Xie and Wei reported the successful levitation of small living animals such as
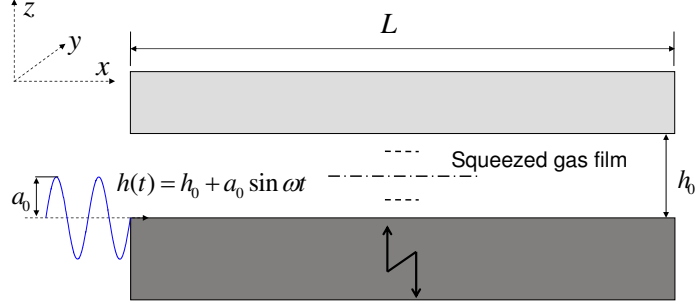
Figure 2.2: Schematic diagram of squeeze film levitation system

ant, ladybug, and little fish with a standing wave acoustic levitator (62). Their experiments showed that the vitality of the small animals was not impaired during levitation.

All the standing wave levitation systems presented above possessed the classic radiator-reflector configuration. The applications of such configuration were limited to the levitation of small particles whose dimension does not exceed the wavelength of the imposed sound wave. Moreover, the levitation force can be obtained from this configuration is very limited. Therefore, modifications and improvements are needed before standing wave ultrasonic levitation can be applied for non-contact suspension systems such as linear and rotational bearings.

2.2.2 Squeeze film type

In 1964, Salbu (47) reported a levitation system for objects with flat surface. Salbu used magnetic actuators to excite two conforming surfaces oscillating next to each other to generate a positive load supporting force. In 1975, Whymark (60) reported that a brass planar disk of 50 mm in diameter and 0.5 mm in thickness was levitated extremely close to a piston vibration source driven harmonically at a frequency of 20 kHz. The levitation effect reported by Salbu and Whymark is named as squeeze film levitation and also called near field acoustic levitation.

A schematic diagram of squeeze film levitation system is shown in Fig. 2.2. The time-averaged mean pressure in the gap has a value which is higher than the surrounding, caused by the second-order effects possessed by the rapidly squeezed and released gas film between two plane surfaces. Two distinct properties distinguish this type of lev-

itation from standing wave levitation. First, the reflector is no longer needed; instead, the levitated object itself acts as an obstacle for the free propagation of the ultrasonic wave-front. Second, the gap between radiation source and the levitated object must be much smaller than the sound wavelength in air. Thus, instead of a standing wave, a thin gas film is formed between the radiator and the levitated object, which is rapidly squeezed and released.

A simple model introduced by Wiesendanger (61) is presented in the following to demonstrate the basic idea of how the squeeze film levitation works. The leaking and pumping at the boundary is neglected in this model. Only the trapped gas which is rapidly squeezed and released is considered. Thus the total mass of air in a fixed volume remains constant, resulting in

$$pV^n \sim ph^n = \text{const.} \tag{2.9}$$

where p represents the pressure, V the volume of the trapped gas, h the gap distance and n the polytrophic constant (n = 1 for isothermal condition, $n = k \approx 1.4$ for adiabatic condition and air). The relation between pressure and levitation distance is nonlinear, which leads to a distorted pressure $p(t)$ resulting from the imposed periodic gap distance $h(t)$. Considering the case shown in Fig. 2.2, the gap distance oscillates harmonically around a equilibrium position h_0, i.e.

$$h(t) = h_0(1 + \epsilon \sin \omega t) \tag{2.10}$$

in which ω is the angular frequency of the oscillation, ϵ the excursion ratio ($\epsilon = a_0/h_0$). The excursion ratio denotes the ratio of the vibration amplitude over the mean gap distance, where a_0 is the vibration displacement amplitude. The mean pressure under isothermal condition ($n = 1$) can be expressed as (61)

$$\bar{p} = \frac{p_0 h_0}{2\pi} \int_0^{2\pi} \frac{1}{h(t)} d(\omega t) = \frac{p_0}{\sqrt{1 - \epsilon^2}} \tag{2.11}$$

It can be easily seen that a mean pressure $\bar{p}$ which exceeds the ambient pressure p_0 is obtained. The result is illustrated in Fig. 2.3. The harmonic motion of the radiating surface produces a non-harmonic pressure oscillation whose mean value is not equal to the quasi-static value p_0. The positive mean pressure p which is larger than the
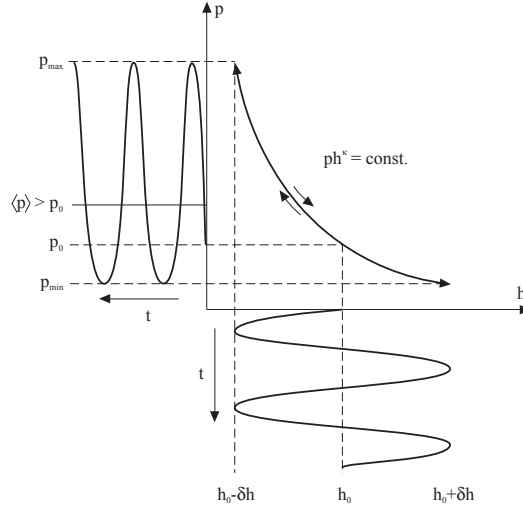
Figure 2.3: The non-harmonic pressure oscillation caused by a harmonic motion (61)

ambient pressure p_0 is clearly shown.

Fig. 2.3 shows qualitatively the existence of a levitation pressure. However, to obtain a quantitative result of the levitation pressure, more sophisticated models should be build which take into account the boundary conditions such as the pressure release at the edge of the gap. The model of squeeze film levitation can be established by following two different routes: acoustic radiation pressure theory and gas film lubrication theory (36). The first one modifies the acoustic radiation pressure theory (will be discussed in Chap. 4) according to the different physical conditions in squeeze film levitation; the second one starts from the theory of gas film lubrication since the working principle is actually similar. Gas film lubrication has been investigated for many years in micro-mechanical systems commonly by solving Reynolds equation (18).

In 1996, Hashimoto et. al. (21) derived a simplified equation for the radiation pressure in squeeze film acoustic levitation from the acoustic radiation pressure theory presented by Chu and Apfel (10). Chu and Apfel calculated the Rayleigh radiation pressure in an ideal gas on a perfectly reflecting target as:

$$p = \langle P - P_0 \rangle = \frac{1 + \gamma}{2} \left(1 + \frac{\sin(2kh)}{2kh} \right) \langle E \rangle \tag{2.12}$$

13

Here, E is the energy density which can be expressed as

$$E = \left(\alpha_0^2/4\right)\left(\rho_0\omega^2/\sin^2 kh\right) \tag{2.13}$$

in which k represents the wave number, γ a specific heat ratio, ω the angular velocity of the wave, a_0 the vibration amplitude and h the distance between vibration source and target. In squeeze film levitation, the levitation distance is very small compared to the wavelength of sound in the free field. It ranges from several to several tens micrometers, therefore $\sin kh \approx kh$. Eq. (2.12) was simplified to a linear equation for the radiation pressure in squeeze film levitation:

$$\Pi = \frac{1+\gamma}{4}\rho_a c^2 \frac{a_0^2}{h^2} \tag{2.14}$$

The radiation pressure Π in squeeze film levitation is reversely proportional to the square of the levitation distance and proportional to the square of the vibration amplitude a_0. Hashimoto did experiments to verify Equ. (2.14). The experimental results of maximum levitation force were 25 percent lower than the calculation results from eq. (2.14). The author supposed that this discrepancy might be due to the finite dimension of the surfaces and the non-uniformity of the amplitude of the radiation surface.

In 2001, Wiesendanger (61) followed the gas film lubrication theory (18; 36) and resolved the general Reynolds equation both analytically and numerically to achieve quantitative results for the levitation forces. In 2002, Nomura and Kamakura (39) theoretically and experimentally examined the squeeze film acoustic levitation. By numerically solving the basic equations of a viscous fluid by means of MacCormack's finite-difference scheme, viscosity and acoustic energy leakage were included in the model. In 2003, Minikes (38) studied the levitation force induced by pressure radiation in gas squeeze films. He investigated the flow induced by vibrations perpendicular to a flat surface and by a flexural wave propagating parallel to the surface. For the first case, numerical and second order analytical perturbation solutions were compared and proved to be in good agreement to each other. For the second case, a modified Reynolds equation was derived to obtain the pressure distribution and the velocity profile in the film for determining the reaction forces. Later in 2006, Minikes examined the validity of the pressure release boundary condition and the isothermal assumptions by a CFD scheme (37). By comparing his results to a one-dimensional analytical solution, the
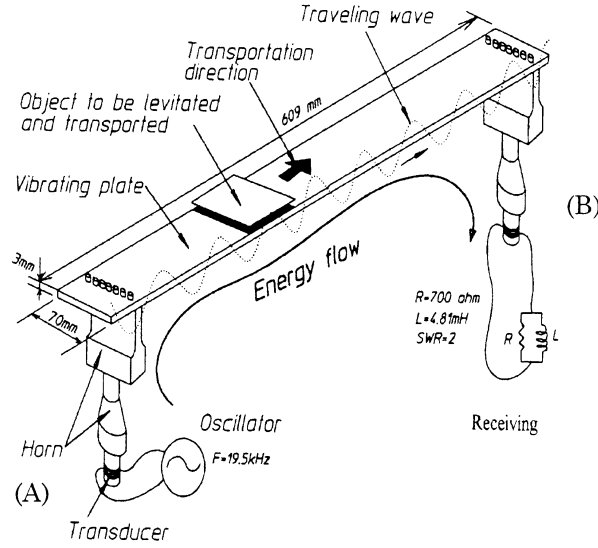
Figure 2.4: Configuration of the transportation system ([20])

author found that the levitation force reduced to a half when the energy leakage near the edges of the levitated object was taken in to account. This indicates that the assumption of pressure release at the boundaries, implied in the Reynolds equation, is inadequate in cases where the driving surface is sufficiently larger than the levitated surface.

The important application of squeeze film levitation is to develop non-contact linear and rotational bearings. This is the major concern of the present thesis and will be discussed in detail in a separated section later. Besides non-contact bearings, squeeze film levitation was also used for non-contact transportation systems. In 1998, Hashimoto ([20]) presented a non-contact transportation system using flexural traveling waves. Fig. [2.4] shows the configuration of the experimental setup. An aluminum plate is connected to two longitudinal transducers and is driven in a flexural vibration mode by one of the transducers. In order to obtain a traveling wave, one transducer acts as vibration source and the other one as a receiver. The transportation speed can be changed by controlling the vibration amplitude. Parallel combination of the systems can provide transportation of wide objects. In, 2000, Amano et. al. ([3]) proposed a squeeze film

levitation system for large-size planar objects. The presented system was an extension of Ueha's transportation system by synchronizing multiple sets of transportation system according to the size of the objects to be transported.

2.3 Non-contact bearings using squeeze film ultrasonic levitation

To overcome the difficulties that are inherent to the existing non-contact bearings, novel concepts for non-contact bearing are consistently of great interest. As one of the promising alternative solutions, squeeze film levitation has been widely investigated for building non-contact linear and rotational bearings. In principle, squeeze film bearing should have most of the advantages of aerostatic bearings. Instead of pressurized air fed through orifice or porous carbon/metal in aerostatic bearings, the load-carrying air film is generated by high frequency vibrations and the corresponding squeeze actions between two surfaces. External pressurized air supply is no longer needed. This feature allows the bearing interface to be as simple as two plain surfaces. The additional effort needed in this kind of bearing is to bring in high frequency vibration to the bearing surfaces. Several prototype non-contact suspension and transportation systems based on squeeze film levitation have been reported in the last decades.

In 1964, Salbu(47) first described the concept of constructing a non-contact bearing using squeeze film action. Salbu used magnetic actuators to generate the oscillation and the operating frequency was in the audible range, therefore the bearing was extremely loud. In the later publications on squeeze film levitation, piezoelectric transducers in various shapes were commonly used to generate the squeeze action effectively. Several designs of squeeze film bearings using bulk piezoelectric ceramics can be found in early U.S. patents filed in 1960s, invented by Warnock (56), Farron (14), Emmerich (13). These designs used bulky piezoelectric materials to create uniform vibration amplitude over the entire bearing surfaces. Therefore the transducers were rather massive and required high power to generate sufficient vibration amplitude. Scranton (48) suggested using bending piezoelectric elements to excite a flexural vibration mode of the bearing. This led to a very compact system design and much lower power dissipation. However,
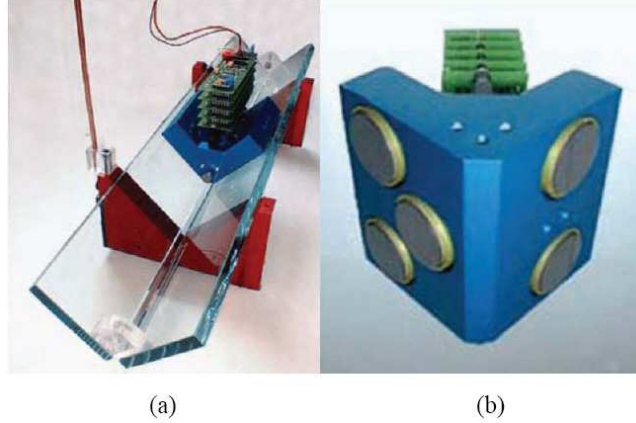
Figure 2.5: Linear slider bearing: a) complete system with glass rail; b) bottom view of the slider with five bearing elements (61)

in Scranton's patent, only the basic concept is sketched, and there was no concrete implementation presented.

Wiesendanger (61) developed a linear guide using disc shape piezoelectric bending elements. The transducers are placed in the sliding part. The carriage which can move freely in a V-shaped rail made of two glass plates is shown in Fig. 2.5 (a). Five disk-shaped piezoelectric bending elements are mounted on the carriage as shown in Fig. 2.5 b. These elements directly constitute the bearing surface, resulting in a highly compact overall design. Wiesendanger also presented a rotational bearing using a tube shape piezoelectric bending element, as shown in Fig. 2.6. Both devices were operated in a resonant frequency in the ultrasonic range. Non-contact suspension was successfully realized. Since the vibration of a bending element is sensitive to load, the vibration amplitude decreases when load is applied on the surface. Therefore, the load capacity of such kind of bearing is always rather limited.

In 2003 Ide et. al. (26) presented a linear bearing based on squeeze film levitation. To hold the lateral position of the slider, a beam with an "L"-shaped cross-section was used as a guide rail, and a slider of the same cross-section is levitated by ultrasonic bending vibrations excited along the beam. Fig. 2.7 shows the configuration of the proposed non-contact linear bearing. A flexural traveling wave is excited along the "L"-shaped beam, and the slider with grooves of the same cross-section is levitated
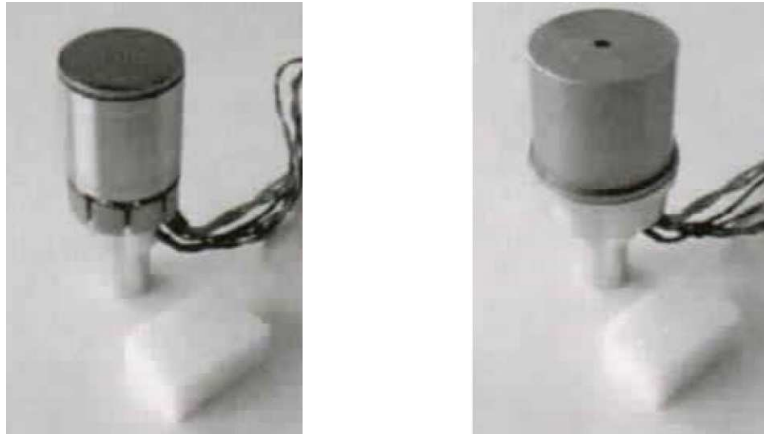
Figure 2.6: Squeeze film bearing, with (right) and without (left) rotor (61)
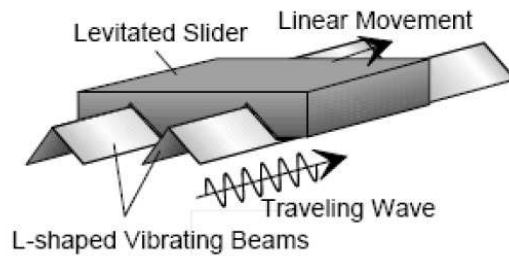
Figure 2.7: A non-contact linear bearing using L-shaped vibrating beams (26)

and moved.

In a further study by Koyama et.al (29), the profile of the sliding table was re-designed using FEM for high levitation and transportation efficiency (see Fig. 2.8). Two bolt-clamped Langevin transducers are used to excite the flexural vibration mode of the sliding guide. The levitation force and levitation capacity were measured to be 4800 N/m^2 and 2500 N/μm/m^2 respectively for a vibration amplitude of 1 μm and a levitation distance of 2.2 μm.

Yoshimoto (65) introduced the use of elastic hinges in squeeze film bearing design and presented a squeeze-film gas bearing with elastic hinges for linear motion guide. Stolarski (51) followed Yoshimoto's idea and developed a self-lifting linear air contact using elastic hinges (see Fig. 2.9). Both Yosimoto (65) and Stolarski (51)'s devices

18
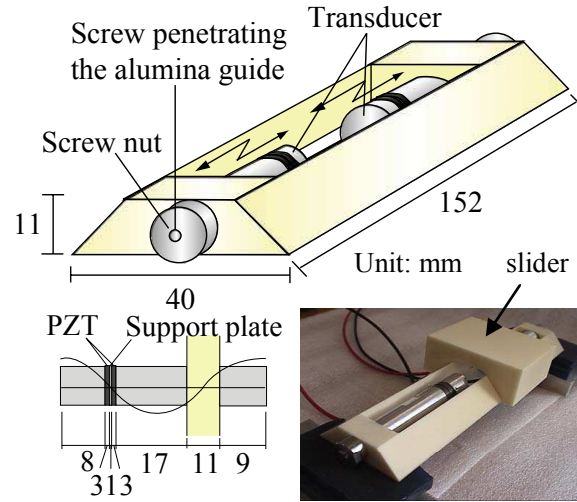
Figure 2.8: Illustration of the ultrasonically levitated sliding table made of alumina ceramics designed by the FEM (29)
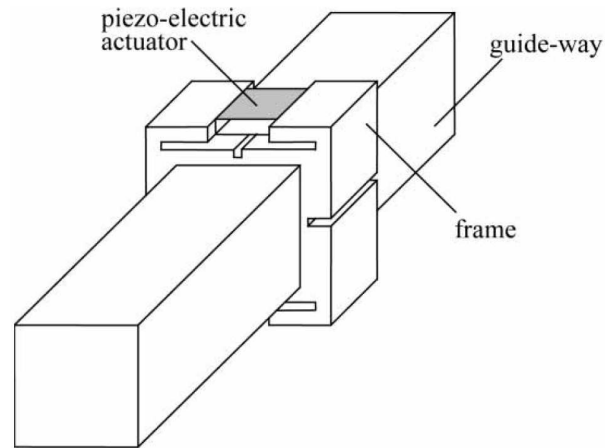
Figure 2.9: Layout of the linear motion bearing (51)
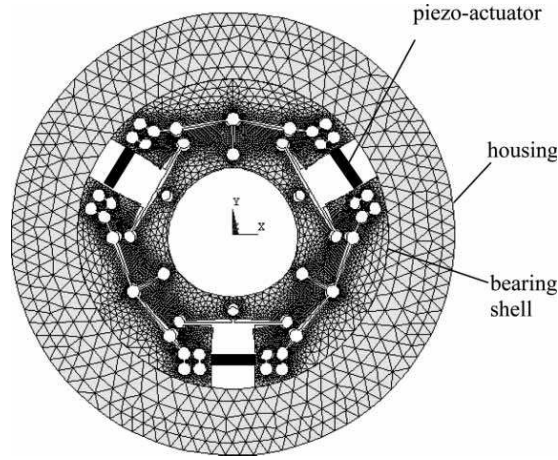
Figure 2.10: Squeeze film bearing using elastic hing, deformed state (17)

were operated at several kHz, out of the resonance of the piezoelectric transducer or the bearing structure. Therefore loud noise can be heard during operation. The obtained vibration amplitudes were also small (few micrometers). This leads to a strict machining tolerance of the bearing and a limited load capacity. In 2007, Yosimoto (66) introduced a new design of the earlier presented linear motion guide (66). The bearing plate was excited to vibrate in a bending mode at ultrasonic frequency by two piezoelectric transducers placed on top of the plate. The newly designed bearing was found to be quiet and have higher load capacity up to 10 N. Ha (17) presented an aerodynamic journal bearing capable of self-lift using squeeze film pressure. The basic principle was the same as Yoshimoto (65) and Stolarski(51)'s design, using elastic hinges and piezoelectric actuators to deform the bearing surface (see Fig. 2.10). The difference was that the bearing has a cylindrical inner surface. During the start and stop, the squeeze film pressure was generated by oscillating the bearing clearance to lift up the spindle; when the spindle reached sufficiently high rotation speed, a three-lobe clearance was formed by deforming the bearing's inner surface using bias voltage applied to the transducers. The bearing could then work as a normal aerodynamic bearing. The load capacity of this bearing was found to be limited at 2.18N, with bearing clearance and frequency of 0.45 μm and 1400 Hz.

According to the model and experimental result presented by Hashimoto et. al.

(21), squeeze film ultrasonic levitation can provide considerably high levitation capacity of about 7 N/cm^2, which is comparable to common air bearings which normally have load capacity in the range of 10 to 20 N/cm^2. However, in practice, the load capacity is restricted by many factors such as the performance of the ultrasonic transducer, the energy efficiency, the limitation of the dimension and so on. The previously reported squeeze film bearings all had very limited load capacities which are much lower than the load capacity measured by Hashimoto et. al. (21) with a piston vibration source. Up to date, the maximum load capacity per unit area of a squeeze film bearing was achieved by the linear air bearing presented by Yosimoto (66), which is about 1 N/cm^2. The load capacity of the previous squeeze film bearings is inadequate for most practical applications. Therefore, it is of great importance to improve the load capacity of the squeeze film bearings.

3

Research objective and thesis outline

3.1 Research objectives

The goal of the present thesis is to provide a guideline of how to apply ultrasonic levitation technique to develop non-contact suspension systems with high load capacity. As discussed in the preceding chapter, ultrasonic levitation has good potential to be applied in non-contact bearing systems. Squeeze film type ultrasonic levitation has already been applied to develop non-contact bearings by several researchers. However, the load capacity achieved by the existing prototypes is still low and inadequate for many applications which require high load capacity. In the current thesis, squeeze film type ultrasonic levitation will be investigated theoretically to find the crucial design parameters and to improve the levitation capacity. The theoretical model will be validated using experimental results. A novel non-contact journal bearing will be developed based on the theoretical investigation, which aims on high load capacity. The proposed bearing should have comparable performance as other types of non-contact bearings such as conventional air bearing.

Surprisingly enough, standing wave type ultrasonic levitation has not found technical applications in non-contact bearings. This is mainly due to the fact that the conventional radiator-reflector structure for levitation of small particles has very limited load capacity and can only levitate elements which are smaller than the sound

wavelength. In this thesis work, we present a configuration which levitates a planar object which corresponds to the "reflector" in the conventional configuration by forming a standing wave field. In other words, the reflector is the levitated object. The configuration will be able to levitate large planar objects at certain positions at which a standing wave is formed by the radiator and the levitated planar object. Such a levitation system can be applied to build non-contact bearings for applications which require low load capacity but very high separation distance. The theoretical model for the proposed levitation system will be established. A prototype system will be developed to validate the proposed method. To the best of the author's knowledge, this is the first detailed investigation of levitation systems of this type.

3.2   Thesis outline

Chap. 2 discusses the state of the art of ultrasonic levitation and its application in non-contact suspension. Chap. 4 and 5 provide the fundamentals of acoustics theory and the basics of piezoelectric ultrasonic transducer. The knowledge is essential to understand the context in the further chapters about ultrasonic levitation systems.

Chap. 6 and 7 focus on the standing wave type levitation system. In Chap. 6 the conventional standing wave levitation is reviewed first, and followed by a novel configuration which improves the levitation capacity and make it suitable for suspending large planar objects. A prototype system for suspension of large planar objects using the proposed configuration will presented in Chap. 7.

Chap. 8 and 9 focus on the squeeze film type levitation. The basic working principle of squeeze film levitation is presented in Chap. 8. Mathematical models for predicting the levitation force will be presented. The proposed models are validated using experiment results. Once again, a prototype system will be presented in Chap. 9. The prototype system is a non-contact journal bearing for rotating elements such a machine spindle. Design and performance of the proposed bearing will be investigated and presented in this chapter.

To conclude, a summary of the achieved results and an outlook on future work is given at the end.

4

Basic theory on acoustics

The study of high-power acoustic effects on acoustic levitation requires certain knowledge of acoustics and ultrasonics.Therefore, the basic principles of ultrasonics including the propagation of low and finite amplitude waves in fluids will be introduced in this chapter. Nonlinear effects such as radiation pressure and increased absorption will also be discussed.

4.1 Linear theory

4.1.1 Elastic waves in fluids

To describe the wave motion, one has to establish the relationship between the disturbance (i.e. the displacement of the medium particles from their equilibrium positions), time, and distance from the source of the oscillations. Sound waves traveling in gases (air) represent an alternating flow and obey the laws of hydrodynamics. If viscosity and thermal conductivity are neglected at the outset, a complete set of hydrodynamic equations can be written as (2; 46):

$$\rho \frac{D\vec{v}}{Dt} = -\nabla p + \vec{g}\rho \tag{4.1}$$

$$\frac{D\rho}{Dt} + \nabla \cdot (\rho \vec{v}) = 0 \tag{4.2}$$

$$f(P, \rho, T) = 0 \tag{4.3}$$

in which, p represents the pressure, ρ the medium density, $\vec{v}$ the velocity vector, T the absolute temperature, and $\vec{g}$ the acceleration vector due to gravity. The convective time derivative $\frac{D}{Dt}$ is a derivative taken with respect to a moving coordinate system, which is given by

$$\frac{D}{Dt} = \frac{\partial}{\partial t} + \vec{v} \cdot \nabla \tag{4.4}$$

where ∇ is the gradient operator.

Equ. 4.1 is called Euler equation which describes the motion of particles subjected to a pressure gradient and gravity forces. Equ. 4.2 is known as the equation of continuity which is valid if there are no discontinuities in the medium, as in the absence of cavitation. Equ. 4.3 is the equation of state, which provides a mathematical relationship between the state functions associated with the matter. Its specific form depends on the material properties and the given physical conditions. In many applications of acoustics, it is these equations that are used as a starting point. Due to the convective terms, Equ. 4.1 to 4.3 are nonlinear in the unknowns. The nonlinear equations can be linearly approximated for the case of low-amplitude waves.

4.1.2 Equations of linear acoustics

In the case of low amplitude acoustic waves, changes in density ρ' and pressure p are small as compared with ρ_0 and P_0. In other words:

$$\left| \frac{P - P_0}{P_0} \right| = \left| \frac{p}{P_0} \right| \ll 1 \tag{4.5}$$

$$\left| \frac{\rho - \rho_0}{\rho_0} \right| = \left| \frac{\rho'}{\rho_0} \right| \ll 1 \tag{4.6}$$

The ambient fluid velocity (such as wind in air) may be neglected if it is much less than the sound speed c. The effects of the gravitational force can usually be neglected. Analogous arguments can be made for the thermal conductivity and viscosity. By neglecting gravity and assuming the ambient fluid velocity is zero, the ambient pressure is then constant. In such cases, Equ. 4.2 can be linearized as

$$\frac{\partial \rho}{\partial t} + \rho_0 \nabla \cdot \vec{v} = 0 \tag{4.7}$$

and the Euler equation becomes

$$\rho \frac{\partial \vec{v}}{\partial t} = -\nabla p \tag{4.8}$$

28

A single partial differential equation for the acoustic part of the pressure can be obtained by taking the time derivative of Equ. 4.7 and then using Equ. 4.8 to re-express the time derivative of the fluid velocity in terms of pressure. The resulting equation is

$$\nabla^2 p - \frac{1}{c^2}\frac{\partial^2 p}{\partial t^2} = 0 \tag{4.9}$$

which is the general wave equation of linear acoustics.

A solution of the wave equation that plays a central role in many acoustical concepts is that of a plane traveling wave. The mathematical representation of a plane wave is such that all acoustic field quantities vary with time and with one Cartesian coordinate (usually taken as z) only. For a plane wave traveling in the positive z-direction at a velocity c and a constant angular frequency ω, the acoustic pressure disturbance can be expressed as

$$p = A_0 \, \cos\left[k\left(z - ct\right)\right] = A_0 \cos(kz - \omega t) \tag{4.10}$$

in which, $k = \omega/c$ is the wave number. In complex representation, the pressure can be written as

$$p = \text{Re}\left(A_0 e^{\text{j}(kz - \omega t)}\right) \tag{4.11}$$

where Re indicates the real part of the expression.

4.1.3 Acoustic energy density and intensity

In a plane progressive harmonic wave both pressure and velocity are in phase. Potential and kinetic energy are transported by the wave without transportation of mass. The potential energy density V due to compression of the fluid and the kinetic energy density K of the wave can be expressed as:

$$V = \frac{1}{2}\frac{1}{\rho_0 c^2}p^2 \tag{4.12}$$

$$K = \frac{1}{2}\rho_0 v^2 \tag{4.13}$$

The total energy density E is then

$$E = V + K = \frac{1}{2}\frac{1}{\rho_0 c^2}p^2 + \frac{1}{2}\rho_0 v^2 \tag{4.14}$$

The acoustic intensity $\vec{I}$ is defined as

$$\vec{I} = p\vec{v} \tag{4.15}$$

For a plane wave, the kinetic energy density and the potential energy density are the same, and the total energy density is given by

$$E = \frac{1}{\rho_0 c^2} p^2 \tag{4.16}$$

4.1.4 Atmosphere absorption of sound wave

When a sound wave travels through air, a proportion of the sound energy is converted to heat. There are losses due to heat conduction, shear viscosity and molecular relaxation. The air absorption becomes significant at high frequencies and at long range (46). For a plane wave, the pressure $|\hat{p}|$ at a distance z from a position where the pressure is $|\hat{p}_0|$ is given as

$$|\hat{p}| = |\hat{p}_0|\, e^{-\alpha z} \tag{4.17}$$

The attenuation coefficient α for air absorption depends on frequency, humidity, temperature and atmospheric pressure and may be calculated using the equations given in Refs. (5; 6),

$$
\begin{aligned}
\alpha = f^2 \Bigg\{ &1.84 \times 10^{-11} \left(\frac{T}{T0}\right)\left(\frac{p_{s0}}{p_s}\right) + \left(\frac{T}{T_0}\right)^{-5/2} \\
&\left[0.01278 \frac{\exp(-2239.1/T)}{f_{rO} + f^2/f_{rO}} + 0.1068 \frac{\exp(-3352/T)}{f_{rN} + f^2/f_{rN}}\right] \Bigg\}
\end{aligned}
\tag{4.18}
$$

where f represents the frequency of the wave, p_s the atmospheric pressure, p_{s0} the reference atmospheric pressure, T the atmospheric temperature in K, T_0 the reference atmospheric temperature, f_{rO} and f_{rN} the relaxation frequencies of the molecular oxygen and nitrogen. The relaxation frequencies f_{rO} and f_{rN} can be calculated as

$$f_{rO} = \frac{p_s}{p_{s0}} \left(24 + 4.04 \times 10^4 c_w \frac{0.02 + c_w}{0.391 + c_w}\right) \tag{4.19}$$

$$f_{rN} = \frac{p_s}{p_{s0}} \left(\frac{T_0}{T}\right)^{1/2} \left(9 + 280 c_w \times \exp\left\{-4.17\left[\left(\frac{T_0}{T}\right)^{1/3} - 1\right]\right\}\right) \tag{4.20}$$
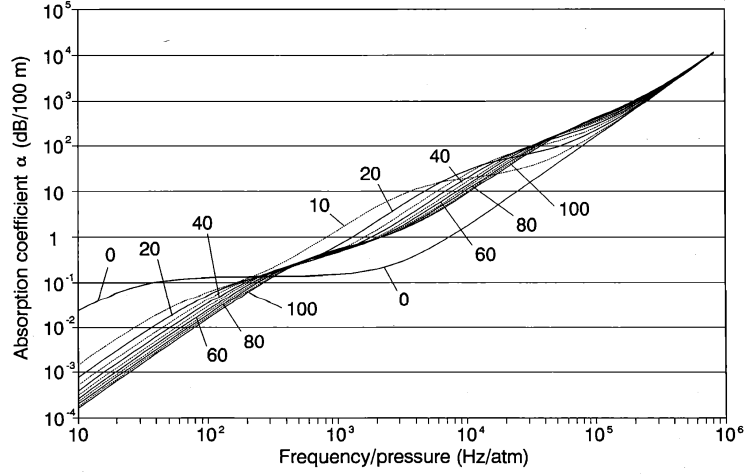
Figure 4.1: Sound absorption coefficient in air (dB/100 m) versus frequency/pressure ratio for various relative humidities (in percent) at 20°C ([5])

respectively, where c_w is the concentration of water vapor in percent. The relation between c_w and relative humidity h_r is

$$c_w = h_r \left(p_{sat}/p_{s0} \right) / \left(p_s/p_{s0} \right) = h_r \frac{p_{sat}}{p_s} \tag{4.21}$$

where the saturated vapor pressure p_{sat} is given by

$$\log_{10} \frac{p_{sat}}{p_{s0}} = -6.8346 \left(\frac{T_{01}}{T} \right)^{1.261} + 4.6151 \tag{4.22}$$

where $T_{01} = 273.16$ K is the triple-point temperature.

Employing the above formulas, the sound absorption coefficient in air versus frequency/pressure ratio was calculated for various percent relative humidity at 20°C by Bass ([5]). The results are plotted in Fig. [4.1].

4.2 Nonlinear theory - acoustic radiation pressure

A body immersed in a sound field is known to experience a steady force that is called the acoustic radiation pressure. This force plays an important role in acoustic levitation. Acoustic radiation pressure is owing to the relative motion of the body and the fluid elements in the medium. Acoustic radiation pressure was first studied by Rayleigh ([44])

in 1902 as an acoustic counterpart of electromagnetic waves. The radiation pressure on the object in the sound field varies with the frequency of the vibrations and equals zero in a linear approximation. A second order approximation is needed to obtain a non-zero pressure, which is small compared with the sound pressure amplitude. Rayleigh found that the acoustic radiation pressure on a perfectly reflecting surface due to a normally incident plane sound wave in an ideal gas is

$$p_{\mathrm{ra}} = \frac{\gamma + 1}{2} \langle E \rangle \tag{4.23}$$

where γ is the ratio of the specific heats of the gas, and $\langle E \rangle$ the time averaged energy density of the standing wave formed by the incident and reflected waves. From these basic equations, the subject has been investigated by many researchers with different results and had been continued to be associated with a lot of confusion for a few decades, mainly because the phenomenon involves a subtle nonlinear effect. Chu noted that the problem has to be very carefully posed in order to get a unique answer (9). In this work, the approach of Lee and Wang (30) is adopted to explain the principles of acoustic radiation pressure.

Euler equation for an ideal fluid is written as

$$\frac{\partial \vec{v}}{\partial t} + (\vec{v} \cdot \nabla) \, \vec{v} = -\frac{\nabla P}{\rho} \tag{4.24}$$

Here $P = P_0 + p$ is the total total pressure, in which P_0 is the ambient pressure and p the acoustic pressure. Since sound oscillation is irrotational, one can write $\vec{v} = \nabla \phi$, where ϕ is the velocity potential. Then Equ. 4.24 can be written as

$$\nabla \left(\frac{\partial \phi}{\partial t} + \frac{1}{2} |\nabla \phi|^2 \right) = -\frac{\nabla P}{\rho} \tag{4.25}$$

The first law of thermodynamics gives (46)

$$\mathrm{d}w = T \, \mathrm{d}S + \mathrm{d}P/\rho \tag{4.26}$$

where T is the temperature, and S and w are the entropy per unit mass and the enthalpy per unit mass of the fluid respectively. Assuming that the motion is adiabatic, one can have $\mathrm{d}w = \mathrm{d}P/\rho$, or $\nabla w = \nabla P/\rho$. Thus Equ. 4.25 can be integrated once in space to give

$$w = -\frac{\partial \phi}{\partial t} - \frac{1}{2} |\nabla \phi|^2 + C' \tag{4.27}$$

where C' is constant in space but can depend on time.

The pressure P can be expanded in Taylor series in w as

$$P = P_0 + \left(\frac{\mathrm{d}P}{\mathrm{d}w}\right)_{s,0} w + \frac{1}{2}\left(\frac{\mathrm{d}^2P}{\mathrm{d}w^2}\right)_{s,0} w^2 + \cdots \tag{4.28}$$

where the subscript $s, 0$ means evaluated at constant entropy and at equilibrium. Since $(\mathrm{d}w/\mathrm{d}P)_s = 1/\rho$, we have then $(\mathrm{d}P/\mathrm{d}w)_s = \rho = \rho_0$, and

$$\left(\frac{\mathrm{d}^2P}{\mathrm{d}w^2}\right)_s = \left(\frac{\mathrm{d}\rho}{\mathrm{d}w}\right)_s = \left(\frac{\mathrm{d}\rho}{\mathrm{d}P}\right)_s \left(\frac{\mathrm{d}P}{\mathrm{d}w}\right)_s = \frac{\rho}{c^2} = \frac{\rho_0}{c_0^2} \tag{4.29}$$

making use of the elementary relation $(\mathrm{d}P/\mathrm{d}\rho)_s = c^2$ and letting all these quantities take equilibrium values. Equation 4.28 becomes

$$P = P_0 + \rho_0\left(-\frac{\partial\phi}{\partial t} - \frac{1}{2}|\nabla\phi|^2 + C'\right) + \frac{1}{2}\frac{\rho_0}{c_0^2}\left(-\frac{\partial\phi}{\partial t} - \frac{1}{2}|\nabla\phi|^2 + C'\right)^2 + \cdots \tag{4.30}$$

By time averaging Equ. 4.30 and keeping up to the second order, we obtain

$$\langle P - P_0 \rangle = -\frac{1}{2}\rho_0\left\langle|\partial\phi^2|\right\rangle + \frac{1}{2}\frac{\rho_0}{c_0^2}\left\langle\left(\frac{\partial\phi}{\partial t}\right)^2\right\rangle + C \tag{4.31}$$

Where C is a constant in space and time. Since it is sufficient to keep up to second order only, in the quadratic terms on the right side of Equ. 4.31 will be sufficiently represented by its linear solution. Substituting $\vec{u} = \nabla\phi$ and $\partial\phi/\partial t = -p/\rho_0$ into Equ. 4.31, we have the mean Eulerian excess pressure as (30)

$$\left\langle P^E - P_0 \right\rangle = \frac{1}{2}\frac{1}{\rho_0 c^2}p^2 - \frac{1}{2}\rho_0 v^2 + C = \langle V \rangle - \langle K \rangle + C \tag{4.32}$$

$\left\langle P^E - P_0 \right\rangle$ is called Eulerian excess pressure because it is evaluated at a fixed point in space, as opposed to the Lagrangian one. The mean Lagrangian excess pressure can be derived from the Eulerian one using the relation between the Lagrangian and an Eulerian quantities (30) as

$$\left\langle P^L - P_0 \right\rangle = \langle V \rangle + \langle K \rangle + C = \langle E \rangle + C \tag{4.33}$$

For 1-D case in general, if the material surface vibrates with the sound, the mean pressure on it is Lagrangian. In the case of a rigid surface, the mean pressure on it becomes Eulerian (30). The mean pressure on the material is the acoustic radiation

pressure. The levitation force can be obtained by integrating the acoustic radiation pressure over the object surface. However, in different types of levitation systems, different boundary conditions and calculation methods are needed. And, the considered levitated objects are very unlike. This will be discussed in detail when the specific type of levitation is concerned in the following chapters.

5

Piezoelectric ultrasonic transducers

The essential requirement to realize any kind of application of high-intensity ultrasound, such as ultrasonic levitation, is the generation and transmission of mechanical vibrations of a certain intensity and frequency. The devices which convert a particular type of energy (electrical or mechanical) into acoustic energy are called ultrasonic transducers. To date, piezoelectric ultrasonic transducers are most widely used in ultrasonic technology. The performance of an ultrasonic levitation system will largely depend on the ultrasonic transducer that is employed in the system. Therefore, the understanding of the working principle and the basic design methods is important for investigating ultrasonic levitation systems. This chapter is dedicated to explain the basic modeling, design and driving methods of piezoelectric ultrasonic transducers, in particular the Langevin type transducers.

5.1   Piezoelectric actuator

5.1.1   Piezoelectric effect

The piezoelectric effect was discovered by Jacques and Pierre Curie in 1880. They found that if certain crystals were subjected to mechanical strain, they became electrically polarized and the degree of polarization was proportional to the applied strain. The Curies also discovered that these same materials deformed when they were exposed to an
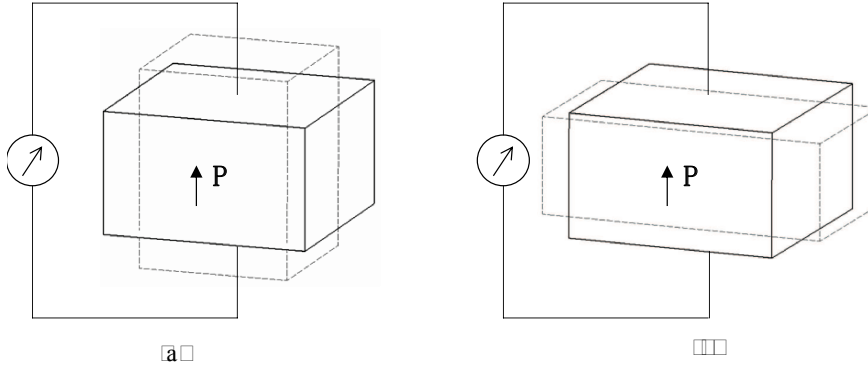
Figure 5.1: Piezoelectric actuators. a), d_{33}, b), d_{31}

electric field. This is known as the inverse piezoelectric effect which is the fundamental for the application of piezoelectric materials in actuators (27).

The electric field deforms a piezoelectric body in different directions with different intensities. For simplicity, only the two most often used types of piezoelectric effects for building piezoelectric actuators are show in Fig. 5.1, namely the longitudinal and transversal deformation due to an applied electric field in the direction of polarization.

As piezoelectric materials are anisotropic, the polarization is done in one direction which is normally given an index of 3, and the directions normal to that with index 1 and 2. When subject to an electrical field in the direction of polarization, piezoelectric element which can deform freely exhibits a strain that can be written as

$$s = E_3 d_{3i} \tag{5.1}$$

in which s represents the resulted strain, E_3 the applied electrical field and d_{3i} the charge constant which has the dimension of m/V. For actuators using the longitudinal effect, the piezoelectric element deforms primarily in the same direction as the applied electric field. As of the transversal effect d_{31}, the deformation is in the direction perpendicular to the direction of applied electrical field. Fig. 5.1 shows the working principle of the two types of piezoelectric effects.

5.1.2 Piezoelectric actuators

Piezoelectric actuators convert electrical energy into mechanical force and motion using piezoelectric elements, most often piezoelectric ceramics. According to the electrical

drive method, they can be divided into two categories: the resonant driven piezoelectric actuators and the non-resonant driven piezoelectric actuators. The resonant driven piezoelectric actuators include e.g. ultrasonic transducers (converters), ultrasonic motors and piezoelectric transformers. The non-resonant driven piezoelectric actuators include various one-stroke actuators. Their operating frequency range is from quasi-static up to about half of the first resonant frequency of the mechanical system.

Typical strain levels that can be obtained by piezoelectric materials are in the region of 0.1%. For quasi-static applications, this strain occurres at field strength in the region of 1000 V/mm. This maximum field strength is limited to approximately 75% of the value of the coercive field. In order to increase the total displacement capability of a piezoelectric actuator, stack and multilayer piezoelectric elements are often used. For resonant driven actuators, another common way to increase the dynamic displacement is to use amplifying mechanisms such as horns and boosters.

5.1.3   Lumped parameter model

The dynamic behavior of a linear system subjected to harmonic excitation can usually be described with sufficient accuracy by superposing only a few of the eigenmodes. Each eigenmode dominates the vibration behavior of the system in the range of the respective resonant frequency. Therefore, if a piezoelectric system is driven in the range of one of its resonant frequencies, its behavior can most often be described with reasonable accuracy by a model with only one degree of freedom.

Based on electro-mechanical analogies the vibration behavior of a piezoelectric actuator operating in the vicinity of one of its resonant frequencies can be described by an equivalent mechanical or electrical model as shown in Fig. 5.2 and 5.3 (33; 54). In the models, m, c, d, C and R are modal mass, modal stiffness, modal damping, electrical capacitance and electrical resistance, respectively. The electromechanical transformation factor α describes the transmission ratio of electrical and mechanical quantities. The input voltage and charge are represented by U and Q. The modal displacement and mechanical load are represented by u and F. According to these models, the dynamics
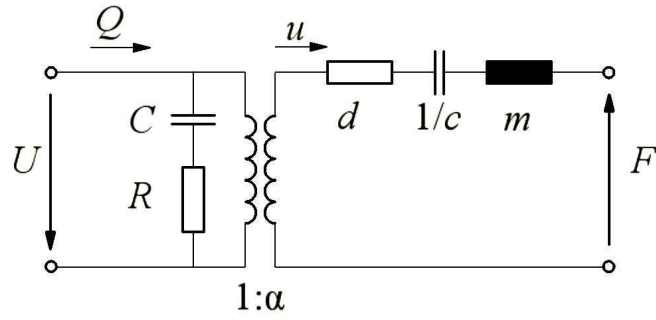
Figure 5.2: The equivalent model for a piezoelectric actuator, electrical representation (54)
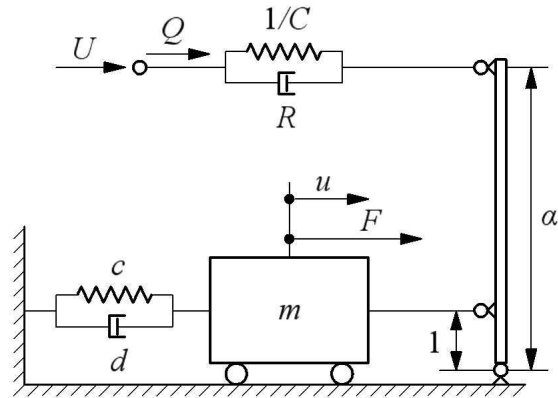
Figure 5.3: The equivalent model for a piezoelectric actuator, mechanical representation (54)

of the system can be described by

$$m\ddot{\underline{u}} + d\dot{\underline{u}} + c\underline{u} = \alpha\underline{U} + \underline{F} \tag{5.2}$$

$$\frac{1}{C}\left(\underline{Q} - \alpha\underline{u}\right) + R\left(\dot{\underline{Q}} - \alpha\dot{\underline{u}}\right) = \underline{U} \tag{5.3}$$

For harmonic excitation $U(t) = \mathrm{Re}[\hat{\underline{U}} \cdot e^{j\Omega t}]$, the relation between inputs and outputs can be written as (22)

$$\begin{bmatrix} \hat{\underline{I}} \\ \hat{\underline{u}} \end{bmatrix} = \begin{bmatrix} \underline{y}_{11} & \underline{y}_{12} \\ \underline{y}_{21} & \underline{y}_{22} \end{bmatrix} \begin{bmatrix} \hat{\underline{U}} \\ \hat{\underline{F}} \end{bmatrix} = \begin{bmatrix} \frac{j\Omega}{jR\Omega + \frac{1}{C}} + \frac{j\Omega\alpha^2}{-m\Omega^2 + jd\Omega + c} & \frac{j\Omega\alpha}{-m\Omega^2 + jd\Omega + c} \\ \frac{j\Omega\alpha}{-m\Omega^2 + d\Omega + c} & \frac{j\Omega}{-m\Omega^2 + jd\Omega + c} \end{bmatrix} \begin{bmatrix} \hat{\underline{U}} \\ \hat{\underline{F}} \end{bmatrix} \tag{5.4}$$

where $\hat{\underline{U}}$, $\hat{\underline{I}}$, $\hat{\underline{F}}$ and $\hat{\underline{u}}$ are complex amplitudes, $\hat{\underline{I}} = j\Omega\hat{Q}$ and $\hat{\underline{v}} = j\Omega\hat{\underline{u}}$. $\underline{Y}$ is the transfer matrix, which is also called the conductance matrix. The elements of the transfer matrix are defined as

$$\underline{y}_{11} = \frac{\hat{\underline{I}}}{\hat{\underline{U}}} = \frac{j\Omega}{jR\Omega + \frac{1}{C}} + \frac{j\Omega\alpha^2}{-m\Omega^2 + jd\Omega + c} \tag{5.5}$$

: the short-circuit input admittance

$$\underline{y}_{21} = \frac{\hat{\underline{u}}}{\hat{\underline{U}}} = \frac{j\Omega\alpha}{-m\Omega^2 + d\Omega + c} \tag{5.6}$$

: the short-circuit core admittance (forward)

$$\underline{y}_{12} = \frac{\hat{\underline{I}}}{\hat{\underline{F}}} = \frac{j\Omega\alpha}{-m\Omega^2 + jd\Omega + c} \tag{5.7}$$

: the short-circuit core admittance (backward)

$$\underline{y}_{22} = \frac{\hat{\underline{u}}}{\hat{\underline{F}}} = \frac{j\Omega}{-m\Omega^2 + jd\Omega + c} \tag{5.8}$$

: the short-circuit output admittance

Figure 5.4 shows the typical variation of the amplitude and phase of the shortcircuit input admittance $\underline{y}_{11}$ as a function of frequency (Bode plot) for a piezoelectric actuator. Figure 5.5 gives the corresponding locus of $\underline{y}_{11}$ in the complex plane (Nyquist plot).

Three pairs of characteristic frequencies can be identified in Fig. 5.5, namely the series and parallel resonant frequencies f_s and f_p, the maximum admittance and minimum admittance frequencies f_m and f_n as well as the resonant and anti-resonant frequencies f_r and f_a. Frequencies f_r and f_a are the frequencies at which the phase of the
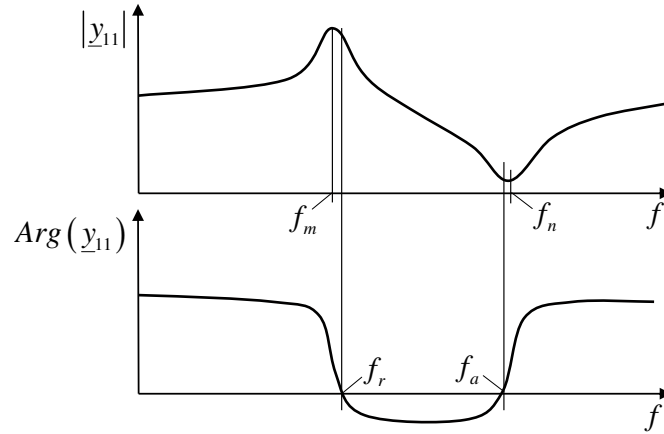
Figure 5.4: Variation of admittance magnitude and phase angle with frequency
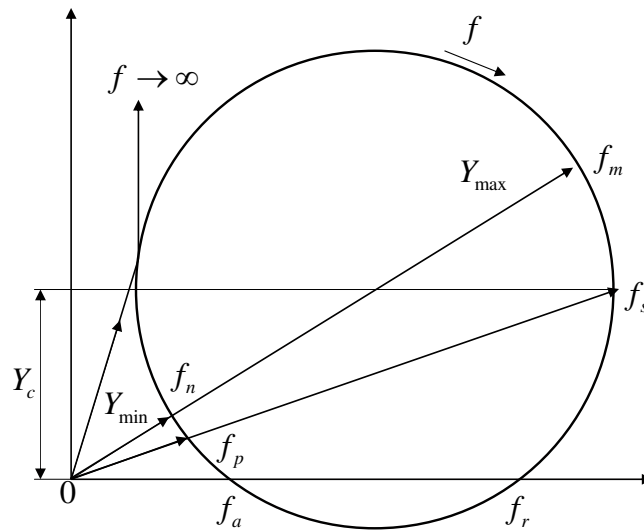
Figure 5.5: Frequency response in the complex plane (22)

Figure 5.6: Typical structure of a Langevin type ultrasonic transducer

admittance becomes zero. For weakly damped systems, $f_m \approx f_r \approx f_s$ and $f_n \approx f_a \approx f_p$.

The model parameters can be calculated from measurement result of admittances. Thus, once the electrical or mechanical admittance of a given piezoelectric system is measured, the dynamic behavior of the system can be precisely described by the model shown in Fig. 5.2 and 5.3 (15; 22).

5.2 Langevin type ultrasonic transducers

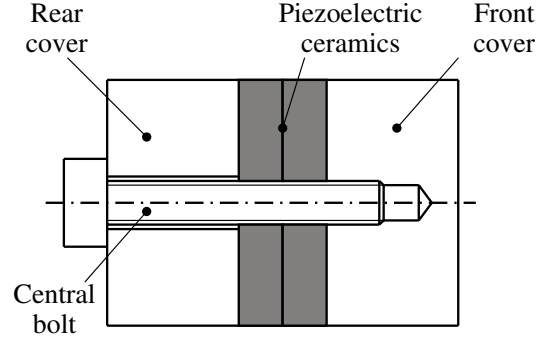For ultrasonic applications, piezoelectric transducers are the most widely used element to generate ultrasonic waves. For power ultrasonic applications such as ultrasonic machining, ultrasonic wire bonding, as well as ultrasonic levitation, the working frequencies are often between 20 kHz and 100 kHz, with high requirements on the power, efficiency and vibration amplitude of the employed ultrasonic transducers. For such applications, Langevin (or sandwich) transducers are often used. A Langevin transducer is composed of head and tail masses, a central bolt for pre-stressing and piezoelectric ceramic rings pressed in the middle. A typical Langevin type transducer is shown in Fig. 5.6.

Langevin transducers have several advantages. Because a mechanical pre-stress is applied on the piezoelectric elements by means of a central bolt or peripheral sleeve, the admissible dynamic stress amplitude and hence the maximum power intensity is considerably increased. The mechanical contact between the parts is improved due to the pre-stressing; hence the mechanical damping is decreased. The metal end sections
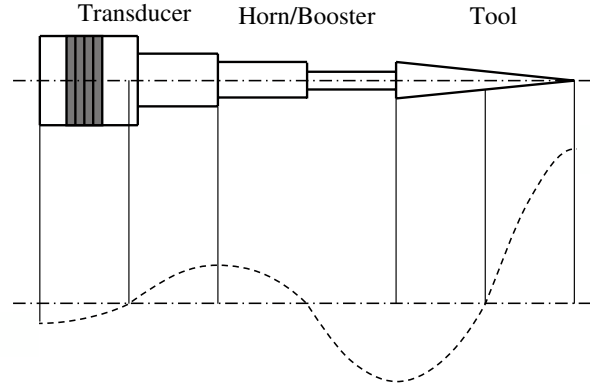
Figure 5.7: The principle of the $\lambda/2$-synthesis

are good heat-sinks, so that the transducer can be driven at higher vibration levels than other types of ultrasonic transducers. As the manufacture of metal is much easier than that of piezoelectric materials, more variations of shape and dimension of transducers are available.

5.2.1 The half-wavelength-synthesis

Langevin transducer is often designed to have length equal to half of the wavelength of the first longitudinal vibration mode of the transducer, often called as $\lambda/2$ vibration mode. The reason is that a $\lambda/2$ transducer can be combined with other $\lambda/2$ parts like boosters or tools to form a whole ultrasonic device without obvious changes of the resonance compared with that of each part before synthesis (33). The advantage of the $\lambda/2$-synthesis is that in the ideal case no forces act at the interfaces between individual parts. Therefore, the boundary conditions of each part in the whole synthesized system are the same as those of each part free at both sides. Under this condition, each part (transducer, booster or tool) can be first developed according to the specified resonance frequency and then they are synthesized into a whole device. Figure 5.7 describes the $\lambda/2$-synthesis principle schematically.

5.2.2 Dimensioning method

To design a Langevin type ultrasonic transducer a lot of design parameters and aspects have to be considered, such as working frequency, radial dimensions, amount of piezo-ceramics, materials for front and rear covers, output power, impedance matching and
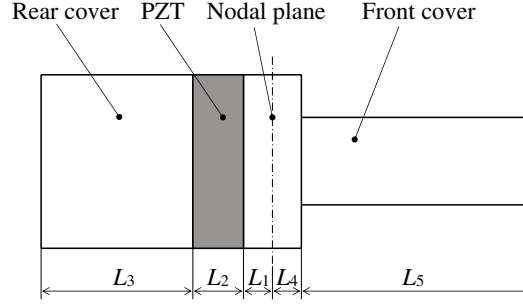
Figure 5.8: Design of the power ultrasonic transducer with nodal plane inside of the front cover

so on. Many of these parameters are determined by the requirement of specific applications. The detailed design method can be found in Refs. 1; 43; 49. Here, a simple case is demonstrated in which all parameters are fixed except the axial lengths L_1, L_2 $\cdots$, L_5. A schematic diagram of the transducer is shown in Fig. 5.8. The nodal plane of the transducer is designed to be within the front cover, so that the transducer can be modeled as two individual 1/4 wavelength systems divided by the nodal plane. Consider the longitudinal vibration of a thin bar with uniform cross section, the frequency equation of the 1/4 wave length transducer on the left side of the nodal plane can be written as (43):

$$\frac{z_3}{z_2} \tan k_2 L_2 \tan k_3 L_3 + \frac{z_3}{z_1} \tan k_1 L_1 \tan k_3 L_3 + \frac{z_2}{z_1} \tan k_1 L_1 \tan k_2 L_2 = 1 \qquad (5.9)$$

The equation for the stepped horn on the right side of the nodal plane can be written as:

$$\tan k_4 L_4 \tan k_5 L_5 = \frac{z_4}{z_5} \qquad (5.10)$$

in which, z_i, k_i, L_i, $(i = 1, 2, 3, 4, 5)$ are the impedances, wave numbers and lengths of each part of the transducer respectively.

$$z_i = \rho_i c_i S_i \qquad (5.11)$$

in which ρ_i, c_i, S_i, $(i = 1, 2, 3, 4, 5)$ are the density, sound speed and area of cross-section of each part of the transducer. Unknown lengths of the transducer parts can be calculated directly form the above two equations.

43

5.2.3 Performance criteria

The performance of piezoelectric transducers is evaluated by different criteria according to different applications. For the power ultrasonic transducers, the most commonly performance criteria are collected here.

- Resonance frequency

The resonance frequency of the transducer should be equal to the specified working frequency. Commonly, this resonance frequency is that of the first longitudinal vibration mode.

- Input/output power

The input power $p_\mathrm{e}(t)$ of the transducer is given as

$$p_\mathrm{e}(t) = U(t) \cdot I(t) \tag{5.12}$$

where $U(t)$ and $I(t)$ are the AC input voltage and current respectively. When the system is not driven in a region around the resonant frequency, it will show a capacitive behavior. The mean effective power is given by

$$P_\mathrm{e} = \frac{1}{T} \int_0^T U(t)I(t)dt \tag{5.13}$$

In case of harmonic $U(t)$ and $I(t)$ the effective power results as

$$\hat{P}_\mathrm{e} = \frac{1}{2}\hat{U}\hat{I}\cos\phi_\mathrm{e} = \hat{P}_\mathrm{a}\cos\phi_\mathrm{e} \tag{5.14}$$

where $\hat{P}_\mathrm{a}$ is the apparent power, ϕ_e is the phase difference between $U(t)$ and $I(t)$. The apparent power determines the size of the power electric device used to drive transducers. Therefore, in order to reduce the size of the power electric device, the apparent power should be minimized for a given output requirement such as a given amplitude or mechanical power.

The mechanical output power of a transducer can be calculated as

$$p_\mathrm{m}(t) = F(t) \cdot v(t) \tag{5.15}$$

The effective power for harmonic vibrations can be calculated by analogy with the electrical one as

$$\hat{P}_{\mathrm{m}} = \frac{1}{2}\hat{F}\hat{v}\cos\phi_{\mathrm{m}} = \hat{P}_{\mathrm{a}}\cos\phi_{\mathrm{m}} \tag{5.16}$$

where $\hat{P}_{\mathrm{a}}$ is the apparent power, ϕ_{m} is the phase difference between $F(t)$ and $v(t)$.

- Efficiency and power efficiency

The efficiency η is defined as a ratio of the output mechanical energy to the consumed electrical energy. For the harmonic vibration of the transducer, η can be calculated as

$$\eta = \frac{\hat{P}_{\mathrm{m}}}{\hat{P}_{\mathrm{a}}} = \frac{\hat{F}\hat{v}\cos\phi_{\mathrm{m}}}{\hat{U}\hat{I}\cos\phi_{\mathrm{e}}} \tag{5.17}$$

The power efficiency λ_{p} can be defined as the ratio between the mechanical energy delivered and the electrical energy absorbed by the transducer. For the harmonic vibration of the transducer, this results in

$$\lambda_{\mathrm{p}} = \frac{\hat{P}_{\mathrm{m}}}{\hat{p}_{\mathrm{e}}} = \frac{\hat{F}\hat{v}\cos\phi_{\mathrm{m}}}{\hat{U}\hat{I}} \tag{5.18}$$

Obviously, the high possible efficiency and power efficiency are desirable for the piezoelectric transducers.

- Mechanical quality factor

The mechanical quality factor Q_{m} is a measure for the resonance rise of the piezoelectric transducer. It can be derived from the 3dB bandwidth of the admittance at f_{s} as

$$Q_{\mathrm{m}} = \frac{f_{\mathrm{s}}}{\Delta f_{\mathrm{s}}(3\text{ dB})} = \frac{f_{\mathrm{s}}}{f_2 - f_1} \tag{5.19}$$

The frequencies f_1 and f_2 are frequencies that correspond to the admittances that are 3dB lower than the maximal admittance, respectively. A large mechanical Q_{m} corresponds to a large efficiency of the piezoelectric transducer and a large resonant amplitude. The material and structural damping of the piezoelectric transducer mainly determine the mechanical quality factor.

- Piezoelectric quality number

According to Fig. 5.5, a piezoelectric quality number is geometrically defined as

$$M = \frac{Y_r}{Y_c} \tag{5.20}$$

where $Y_r = Y_{max} - Y_{min}$ is the diameter of the locus of $\underline{y}_{11}$ as shown in Fig. 5.5, in which Y_{max} and Y_{min} are the values of $\underline{y}_{11}$ at the frequencies f_m and f_n, respectively. The piezoelectric quality number is an important performance parameter. It presents the extent of the phase rise or phase drop of the admittance functions and is appropriate to classifying piezoelectric actuators concerning electrical behaviors. When $M < 2$, the resonance and anti-resonance frequencies do not exist anymore, the transducer can not be driven with zero reactive power. More apparent power is needed which leads to a large power electric device. Therefore, the piezoelectric quality number of the transducer used in ultrasonic bonding and machining should be larger than two. Furthermore, the larger the value of M is, the better the phase reserve of the transducer. When $M > 2$, it is assured that the resonance frequency exists and that the transducer can be driven with zero reactive power even though the load damping may be large (15).

5.3 Driving method

The ultrasonic transducers are resonance driven systems, therefore the driving frequency must match the resonant frequency of the system. It is worth mentioning that the term "resonant frequency" is originally a concept of free vibrations to describe the frequency when the system has large vibration amplitude. For forced vibration, "resonant frequency" is often misused as the frequency when the response amplitude is maximal. It has become an accepted mistake. Therefore, we will also use the term "resonant frequency" in this context to discuss the forced vibration of piezoelectric transducers.

The resonance frequency of every individual transducer varies slightly due to manufacturing tolerances. Moreover, the resonant frequency is also subject to change during operation from change of load, temperature, input power and so on. Therefore, it is necessary to implement a resonance tracking scheme that can adjust the driving frequency during operation. This is especially important when the system has a high mechanical
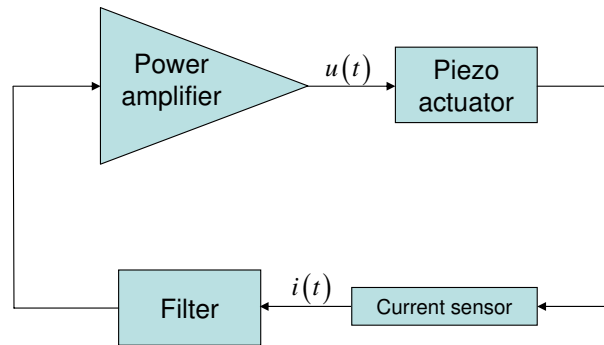
Figure 5.9: Basic scheme of a self oscillating circuit

quality factor Q_{m}. Two widely used resonance tracking methods, self oscillating circuit and Phase Locked Loop (PLL) control, will be introduced here.

5.3.1 Self oscillating circuit

The basic idea of a self oscillating circuit is to make the whole circuit unstable at the desired vibration frequency in such a way that the system develops a limit cycle. To do so, two conditions must be satisfied: first, the feedback must be positive, i.e. the total phase shift in the feedback loop should be zero. Second, the loop gain must be greater than unity so that there is a net amplification within the loop. If these two requirements are met at a certain frequency (eigenmode), a self-induced oscillation will be sustained (61). If, however, the requirements are met at more than one frequency (eigenmode), a filter that is placed in the feedback path will allow to pick the desired one. The basic scheme of a self oscillating circuit is shown in Fig. 5.9.

There are some drawbacks of the self oscillating circuit which make it unsuitable for certain applications such as squeeze film levitation. The efficiency of the system is poor. Moreover, at high power levels and in applications where loading conditions may vary strongly over time, the system becomes highly nonlinear, so that the conditions for instability are not fulfilled any more. As a result, the system will fail to work.

5.3.2 Phase-locked-loop (PLL) controller

The PLL controller is a more robust alternative algorithm to operate piezoelectric transducers in their resonant frequency. The block-diagram of the loop is shown in Fig. 5.10.
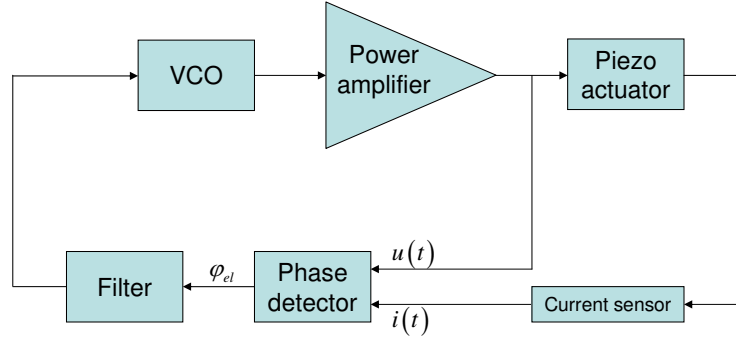
Figure 5.10: Block diagram of phase-locked-loop algorithm

The PLL consists of a phase detection, a filter, a voltage controlled oscillator (VCO), and a current sensor. The piezoelectric actuator (the ultrasonic transducer) is driven by a power amplifier that, in turn, is driven by a voltage-controlled oscillator. The change in output frequency of the VCO from its initial value is proportional to the applied voltage at the input. The inputs to the phase detector are the actual driving voltage and current on the transducer. The phase difference between these two signals must be controlled to be zero to maintain resonance. After the filter, the output of the phase detector is a voltage proportional to the phase difference between the signals. This voltage is proportional to the error between the driving frequency and the resonant frequency and is applied to the VCO to bring the driving frequency toward resonance (50). The desired driving power level is obtain by adjusting the gain of the power amplifier.

The PLL controller is more complicated than the self oscillating circuit, but it provides more stable and reliable operation. Therefore it is more suitable for driving piezoelectric transducers in resonance. However for a highly damped system, in which the minimum phase value of the admittance between resonance and anti-resonance does not fall below the zero-phase line, the PLL will not be able to find the resonant frequency based on the phase measurements. Thus a PLL will also fail to function. In such cases, a load-adaptive phase controller, like the one developed by Littmann (34), can be used as an extension of the conventional PLL controller. The presented APLL controller includes a transducer model and is able to estimate the phase of the mechanical admittance (v/u), which always has a phase zero-crossing, based on

the measurement of electrical admittance. Using the APLL controller, highly damped systems can be controlled to work at the mechanical resonant frequency.

6

Standing wave ultrasonic levitation

Standing wave type levitation is commonly used for levitating of small particles. Thorough theoretical basis and successful applications have been reported over the last decades. However, the size of objects that can be levitated by standing wave levitation is limited to be smaller than the sound wavelength (mm range). This characteristic prevents standing wave ultrasonic levitation from many potential applications in which suspension of larger, heavier objects is needed. In this chapter, a new configuration of standing wave levitation will be introduced which has an improved levitation capacity and has no restriction on the dimension of the objects anymore. The corresponding theoretical model is established for the proposed configuration.

6.1   A configuration for large planar objects

The typical radiator-reflector type standing wave levitation system, as discussed in Chap. 2, has very limited load capacity and strict restrictions on the size of the levitated objects. Modifications and improvements are needed before standing wave ultrasonic levitation can be applied for non-contact suspension systems.

In 2001, Reinhart (45) reported that while measuring the squeeze film levitation force, additional peaks of levitation force at intervals of half wavelengths from the radiation surface were also observed. These additional peaks had much smaller amplitudes
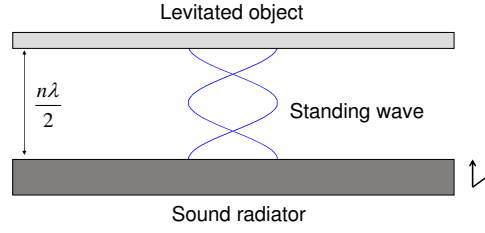
Figure 6.1: Schematic diagram of the proposed acoustic levitation system

($< 0.1N$) compared to the squeeze-film region. Reinhart concluded that they were caused by the standing wave pattern and pointed out a possibility of levitating planar objects at these points. However, no further explanation or experimental investigation was reported afterwards.

In the following parts of this chapter, an acoustic levitation system will presented which uses the levitation effect observed by Reinhart. The levitation happens when planar objects are placed at distances of half wavelengths in front of a radiator. A schematic diagram of the proposed levitation system is shown in Fig. 6.1. In this configuration, the levitation effect is achievable using similar setup of standing wave or squeeze levitation, but the working principle is different in many aspects. First, the acoustic field is formed in between the sound radiator and the levitated object which performs as a reflector as in classic standing wave levitation systems. The position of the object to be levitated determines how the sound field is maintained. Second, the size of the object to be levitated is not limited by the wavelength, because the object is levitated above the complete standing wave field. In the classic standing wave levitation, the small particles are trapped stably slightly under a pressure node or anti-node of a standing wave field formed by a radiator and a reflector. Thus, the particles can only be levitated if they are smaller than a sound wavelength. At last, as compared to squeeze film levitation, the object can be levitated at positions of multiple times of half wavelength above the radiator. A stable levitation happens when a standing wave is formed between the radiator and the object. However, the squeeze film levitation happens only when the object is placed extremely close to the radiator. Thus no standing wave is formed in the gap.

6.2   Modeling the proposed levitation system

The intention of the proposed acoustic levitation system is to levitate planar objects with relative large size (a few times of the sound wavelength in air). In order to obtain a large sound radiation surface, a circular plate which vibrates in its flexural vibration mode is chosen as the sound radiator. The sound field to be considered can be simplified and described as following: the sound radiator (a circular disc) vibrates in its flexural vibration mode and generates a sound beam in front of it. The sound beam propagates forwards and is reflected by a rigid surface (the object to be levitated) placed perpendicular to the sound beam at a distance of L away from the radiator. An acoustic wave field from multiple reflections is formed between two surfaces. The acoustic field becomes a standing wave when L is equal to multiple times of half wavelength of sound (as shown in Fig. 6.1). Excessive pressure on the rigid surface is generated by the acoustic field.

### 6.2.1   Flexural vibration mode of the radiator

The selected sound radiator is a circular plate with constant thickness. Therefore, cylindrical coordinates (r, θ, z) can be used, where r is a radius from the center, θ the angle of that radius, and z a length in the direction normal to the plane of the radiator. The plate equation has the following general solution for the transverse vibration mode of a circular plate (7)

$$Z(r, \theta, t) = \left[a_{ij} \mathrm{J}_i \left(\frac{\lambda_{ij} r}{a} \right) + b_{ij} \mathrm{I}_i \left(\frac{\lambda_{ij} r}{a} \right) \right] \cos i\theta \ \cos 2\pi f t \qquad (6.1)$$

where $Z(r, \theta, t)$ is the displacement of the mid-surface of the plate, a the radius of the circular plate, f the natural frequency of the related mode shape. The subscripts i and j are the number of nodal diameters and nodal circles (not counting the boundary) respectively. Functions J_i and I_i are Bessel function and modified Bessel function of the first kind relatively, of i order. Parameters a_{ij} and b_{ij} are constants which are determined to within an arbitrary constant by the boundary conditions and mode number. The parameter λ_{ij} is a dimensionless frequency parameter related to the boundary conditions on the plate, the plate geometry and Poisson's ratio. For mode shapes with only nodal circles ($i = 0$) the displacement of the circular plate becomes
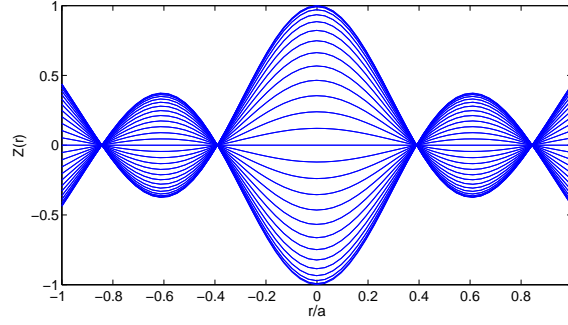
Figure 6.2: Vibration amplitude distribution on the radiator surface

axial symmetric. The displacement Z is then independent of θ. Equation 6.1 can be simplified as

$$Z(r,t) = \left[a_{0j} J_0 \left(\frac{\lambda_{0j} r}{a} \right) + b_{0j} I_0 \left(\frac{\lambda_{0j} r}{a} \right) \right] \cos 2\pi f t \qquad (6.2)$$

The distribution of the vibration amplitude of the mid-surface of the plate can be then given as

$$Z(r) = a_{0j} J_0 \left(\frac{\lambda_{0j} r}{a} \right) + b_{0j} I_0 \left(\frac{\lambda_{0j} r}{a} \right) \qquad (6.3)$$

The vibration mode of a free circular plate with two nodal circles is shown in Fig. 6.2. Values of λ_{ij} of common mode shapes have been calculated and listed in Ref. (7), where λ_{02} is given as 6.209. By applying the boundary conditions, a_{02} and b_{02} are determined as 0.997 and 0.003 respectively.

6.2.2 Sound beam in the acoustic near-field

According to Ref. (49), the acoustic far-field is approximately reached when z exceeds a^2/λ, where a is the radius of the radiator, and λ the wavelength of sound. For the proposed levitation system, the working frequency is about 20 kHz with wavelength λ being about 0.017 m. The radius of the sound radiator is 0.06 m. These makes $a^2/\lambda = 0.208$ m, which is about twelve times of λ. The investigated range of the levitation distance L is around one to a few times of half wavelengths. Therefore the considered sound field is completely located in the acoustic near-field.

A sound beam can be described in cylindrical coordinates with Bessel functions in r and sinusoidal function in z direction (30),

$$p(r, z, t) = A_0 \mathrm{J}(r) \, \cos(\omega t - kz) \tag{6.4}$$

where A_0 is the amplitude of acoustic pressure at $r = 0$, k the wave number, ω the angular frequency of the wave, z the distance from the vibration source and $\mathrm{J}(r)$ the Bessel functions describing the radial distribution of the sound beam. For calculation it is convenient to use a complex number representation. Equation 6.4 can be then written as

$$p(r, z, t) = \mathrm{Re} \left\{ A_0 \mathrm{J}(r) e^{\mathrm{j}(\omega t - kz)} \right\} \tag{6.5}$$

where Re indicates the real part of the expression. In the following Re will not be mentioned for simplification. All the complex parameters are automatically considered as their real parts.

Unlike a plane wave, in a sound beam described by Equ. 6.5, air particles move in both r and z directions. However, in the near-field, the acoustic field is basically cylindrical, the oscillations in the r direction are small compared to z direction and have very little contribution on the radiation pressure. Therefore, the velocity component in r direction is not taken into account in the present model. A sound beam with the same diameter as the radiator is considered. Assuming that the acoustic pressure at the surface of the radiator varies exactly according to the transverse movement of the radiator, the Bessel functions in Equ. 6.5 can be replaced by $Z(r)$. The sound beam in near-field can be then expressed as:

$$p(r, z, t) = A_0 Z(r) \, e^{\mathrm{j}(\omega t - kz)} \tag{6.6}$$

The axial pressure at the center of a sound beam generated by a circular piston varies in the near-field and may have one or more maximums occur along the axis when $ka > \pi$. The pressure variations are extreme for a circular piston because of the high degree of symmetry (49). For the circular plate with flexural mode as shown in Fig. 6.2, the fluctuation of axial pressure amplitude at the center is reduced by the nearly symmetric high and low pressure field on the plate. Therefore, the variation of

the pressure amplitude A_0 is not as significant as the circular piston anymore, and is considered as constant in the near-field for the present model. The particle velocity in z direction is expressed as

$$v_z(r, z, t) = \frac{A_0}{\rho_0 c} \, Z(r) e^{\mathrm{j}(\omega t - kz)} \tag{6.7}$$

6.2.3 Increased absorption due to nonlinear effects

The absorption coefficient α discussed in Sec. 4.1.4 is calculated with linear assumptions. It fits to sound waves with pressure amplitude much smaller than the ambient air pressure ($A_0 \ll P_0$). However, in acoustic levitation systems, high intensity and high acoustic pressure amplitude are normally involved. Propagation of such finite-amplitude waves is accompanied with a variety of nonlinear effects whose intensity depends on the amplitude of vibrations, such as waveform distortion, formation of shock waves, increased absorption, nonlinear interaction, cavitation and sonoluminescence (46). The waveform distortion always exits in nonlinear waves. They come from the generation of higher harmonics during propagation. The absorption increases dramatically for higher frequencies, therefore the distorted wave are absorbed more than the harmonic waves. A relation between the absorption of finite and small amplitude waves is given in Ref. (35) as:

$$\frac{\alpha'}{\alpha} = 1 + \frac{3\omega^2 v_0}{4\alpha c^2} \left(1 + \frac{B}{2A}\right) e^{-2\alpha z} \left(1 - e^{-2\alpha z}\right) \tag{6.8}$$

In which, α' represents the increased absorption coefficient of finite amplitude wave, v_0 the air particle speed amplitude, z the traveling distance. The nonlinearity parameter B/A is parameter for characterizing the strength of the nonlinearity of a medium and $B/A = 0.40$ for air (46). The increased absorption coefficient α' is now a function of the particle speed amplitude v_0 and increases as v_0 gets higher. When standing wave is formed, as a result of signified resonance, the air particle speed increases significantly. As a result, α' obtained from Equ. 6.8 can be significantly larger than α.

By substituting the attenuation coefficient into Equ.6.6 we obtain,

$$p(r, z, t) = A_0 Z(r) \, e^{-\alpha' z + \mathrm{j}(\omega t - kz)} \tag{6.9}$$

6.2.4 Modeling the sound field

Consider the problem in which the sound wave described by Equ. 6.9 traveling in the z direction is reflected at $z = 0$ by a rigid fixed plane wall. The reflected wave is again reflected at the radiation surface located at $z = L$ and propagates toward the reflector. The reflection of the wave goes on and on between two rigid surfaces until the wave is totally absorbed by the air. The resulted sound field between the sound radiator and the reflector is the summation of all the foregoing and reflected waves. The infinite summation of such waves is proved to be equal to the summation of one foregoing and one reflected wave with same amplitude (23). The resulted sound field can be described as

$$p(r, z, t) = A_0 Z(r) \cdot \left(\cos kz \cdot \cosh \alpha' z + \mathrm{j} \sin kz \cdot \sinh \alpha' z \right) e^{\mathrm{j}\omega t} \qquad (6.10)$$

The corresponding acoustic velocity $\vec{v}$ in z direction is expressed as

$$v_z(r, z, t) = -\frac{A_0}{\rho_0 c} Z(r) \cdot \left(\cos kz \cdot \sinh \alpha' z + \mathrm{j} \sin kz \cdot \cosh \alpha' z \right) e^{\mathrm{j}\omega t} \qquad (6.11)$$

Notice that only the near-field region is considered in this context, and the speed of air particles in r direction is ignored. So far, the representation of the entire cylindrical sound field is obtained. The next step is to calculate the radiation pressure produced by the obtained sound field.

Since the reflector surface is considered as rigid, the radiation pressure on it is Eulerian (30). Equation 4.32 can be then applied to calculate the radiation pressure at the reflecting surface generated by the sound field described by Equ. 6.10. Substituting Equ. 6.10 and Equ. 6.11 in to Equ. 4.12 and Equ. 4.13, after time-averaging, $\langle V \rangle$ and $\langle K \rangle$ are obtained as

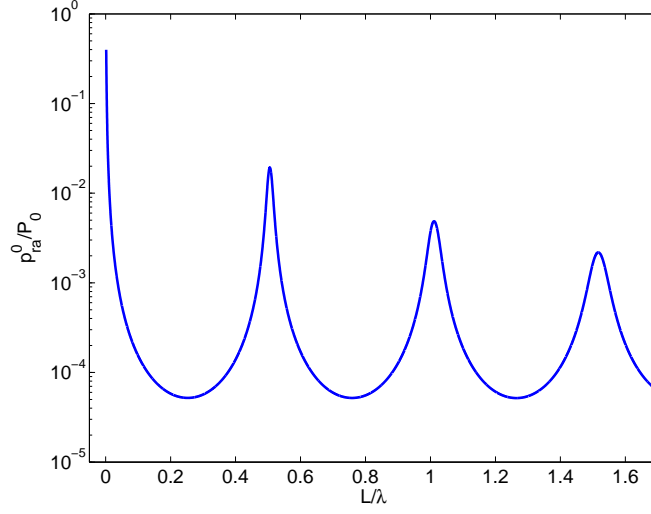$$\langle V \rangle = \frac{A_0^2 Z(r)^2}{4\rho_0 c^2} \left(\cos^2 kz \ \cosh^2 \alpha' z - \sin^2 kz \ \sinh^2 \alpha' z \right) \qquad (6.12)$$

$$\langle K \rangle = \frac{A_0^2 Z(r)^2}{4\rho_0 c^2} \left(\sin^2 kz \ \cosh^2 \alpha' z - \cos^2 kz \ \sinh^2 \alpha' z \right) \qquad (6.13)$$

For a sound beam in free space there is no constrain to satisfy. Therefore, $C = 0$. Substituting Equ. 6.12 and Equ. 6.13 into Equ. 4.32, the mean Eulerian excess pressure is obtained as

$$P^E - P_0 = \langle V \rangle - \langle K \rangle = Z(r)^2 \frac{A_0^2}{4\rho_0 c^2} \cos 2kz \left(\sinh^2 \alpha' z + \cosh^2 \alpha' z \right) \qquad (6.14)$$

Figure 6.3: Change of the radiation pressure at the center of the reflector with different distances

Equation 6.14 describes the mean excess pressure at fixed points within the sound field. For a certain sound field, the mean excess pressure varies at different (r, z) positions. On the plane at $z = 0$ perpendicular to z, the mean pressure becomes the acoustic radiation pressure p_{ra} on the object. The acoustic radiation pressure p_{ra} can be obtained by setting $z = 0$ in Equ. 6.14 as

$$p_{ra} = Z(r)^2 \frac{A_0^2}{4\rho_0 c^2} \tag{6.15}$$

The radiation pressure p_{ra} is not uniform in r-direction and its distribution follows the function $Z^2(r)$

6.3 Simulation results

A normal laboratory condition with temperature of 20 degree Celsius and relative humidity of 30% is assumed for all the calculations in this section. The absorption coefficient α is calculated as 0.58 using Equ. 4.18.

Figure 6.3 shows the radiation pressure changes with different distances between the radiator and the reflector. In the figure, Y axis is radiation pressure at the center of the reflector (p_{ra}^0) caused by the center (near $r = 0$) of the sound beam. The vibration speed amplitude V_0 at the center of the radiator used for this calculation is 3 m/s. In
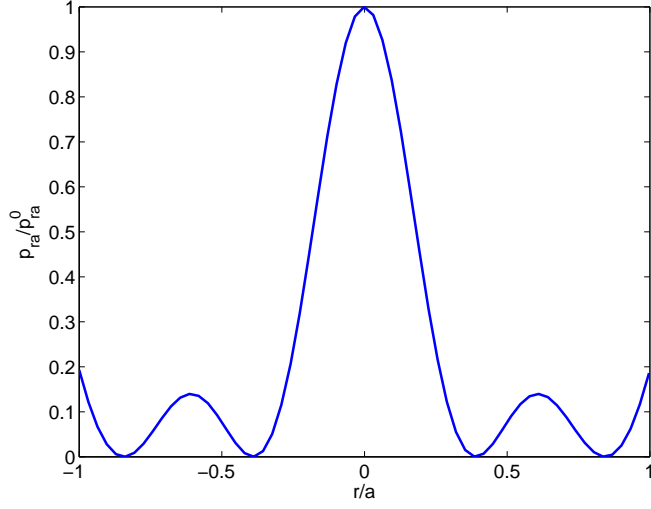
Figure 6.4: Radiation pressure distribution along the surface of the reflector

the figure, p_{ra}^0 is normalized by the atmospheric pressure P_0 and the levitation distance is normalized by the sound wavelength. It can be seen that the radiation pressure is normally very small compared to the atmospheric pressure. However, at intervals of half wavelength, clear peaks happen due to the formation of a standing wave. When L is close to zero, the squeeze film effect takes place, and the resulting pressure increases quickly to a maximum value of 0.4 times of the atmospheric pressure. This corresponds to $V_0 = 3$ m/s.

The distribution of the radiation pressure on a circular surface with $r = 0.06$ m (as in the experiment setup presented in the preceding section) is shown in Fig. 6.4. The radiation pressure p_{ra} is normalized by the radiation pressure at the center of the plate p_{ra}^0. The radial distribution of the amplitude of p_{ra} follows the square of the surface vibration amplitude. At the nodal circles of the radiator, the radiation pressure drops to zero. The levitation force is obtained by integrating p_{ra} along r.

For the proposed acoustic levitation system, it is interesting to know how the frequency affects the levitation force. In order to show the relation, the maximum radiation pressure (at $r = 0$) is calculated with different frequencies. For consistency, the surface vibration velocity is set constantly as $V_0 = 3$ m/s. The vibration speed is an indication of the output power of the radiator. Therefore, it can be considered that
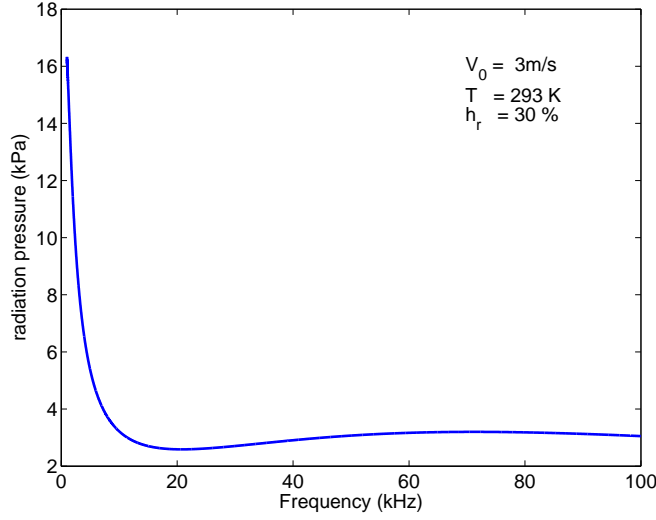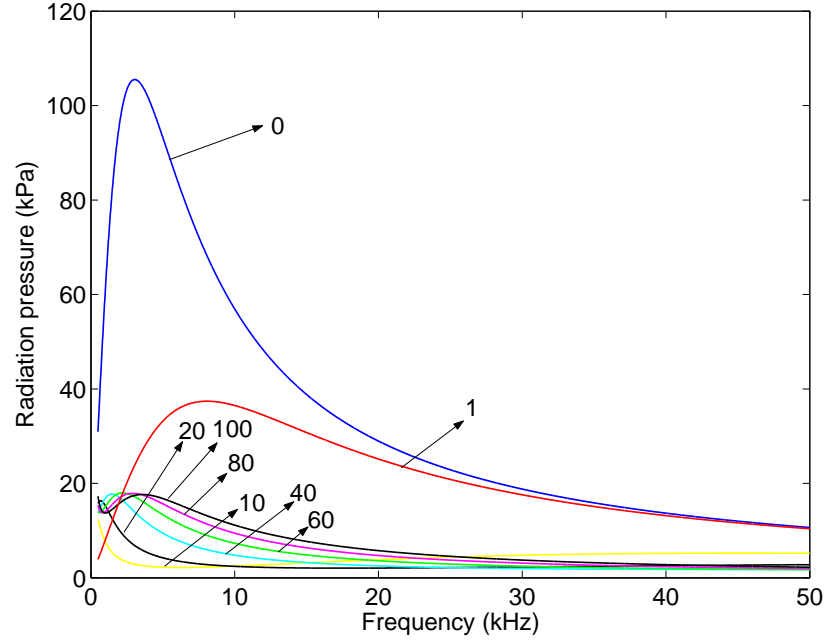
Figure 6.5: Radiation pressure versus frequency, constant vibration speed

the output sound power is kept approximately constant. Fig. 6.5 shows the calculation results. From the figure, one can see that the radiation pressure in the audible range (≤ 20 kHz) increases quickly with decreasing frequency. However, in the low frequency range (≤ 5 kHz), vibration speed of 3 m/s will require a very large displacement of the radiator. This is often not feasible in practice and will be unbearably loud.

It has been discussed earlier that the absorption coefficient is an important parameter which affects the radiation pressure. The absorption coefficient is sensitive not only to the frequency, but also to the humidity (5; 6). Therefore, the humidity should also be considered when performing standing wave levitation. The influence of humidity on the radiation pressure at different frequencies is shown in Fig. 6.6 as an extension of Fig. 6.5. Similarly, the surface vibration velocity is set constantly as $V_0 = 3$ m/s. It can be seen that the radiation pressure increases in general with lower frequency in the audible range. However, for the ultrasonic frequency range (≥ 20 kHz), the radiation pressure is rather not sensitive to the frequency. For very low humidity condition (below 5%), the absorption coefficient α for frequencies higher than 300 Hz decreases severely as can be seen in Fig. 4.1 (5; 6). Such a change of α results in a boost of radiation pressure at extremely low humidity. The results shown in Fig. 6.6 imply that it is necessary to maintain the humidity of the laboratory environment to achieve

Figure 6.6: Radiation pressure versus frequency at different humidities, with constant vibration speed

stable performance of the proposed levitation system.

6.4 Conclusion

A one dimensional acoustic levitation system using ultrasonic standing wave has been discussed in this chapter. To improve the levitation capability of a standing wave levitation system, a different configuration is presented which is able to levitate large planar object (much larger than the sound wavelength) at a position of multiple times of a half wavelength of the sound wave (much higher than squeeze film levitation system). A mathematical model for the system is developed based on acoustic theory. Nonlinear absorption effect is taken into account in the model. The theoretical model gives good insights of the influences of different parameters on the levitation force, such as frequency and vibration mode.

7

Suspension of large planar objects using ultrasonic standing waves

A prototype system will be presented in this chapter which employs the theoretical analysis in the preceding chapter. The proposed system is aimed on suspension of large planar objects at a high levitation distance (in cm range). The experimental setup and the performance of the system will be discussed. Experimental results will be compared with the theoretical results.
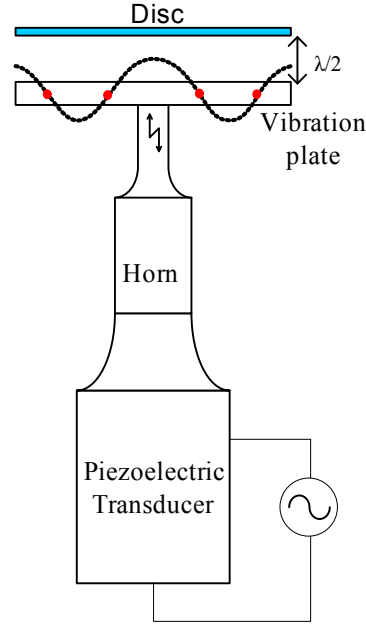
7.1   Experiments

7.1.1   Experimental setup

A schematic diagram of the proposed levitation system is shown in Fig. 7.1. A piezo-electric Langevin type transducer driven in its first longitudinal mode ($\lambda/2$) at 20 kHz is used to generate ultrasonic vibrations. A stepped horn ($\lambda/2$) is attached to magnify the vibration amplitude of the transducer. An aluminum plate of diameter 120 mm is used as sound radiator. The plate is screwed into the horn.

For matching one of the plate's axial symmetric flexural modes of vibration to the axial resonant frequency of horn and transducer, the plate-thickness is chosen so that the corresponding natural frequency of the free-vibrating plate appears at 20

Figure 7.1: Schematic diagram of the experimental setup of the proposed levitation system

kHz (33). Flexural modes of vibration with one, two, and three nodal circles have been constructed by properly matching the thickness. Experimentally, a plate with two nodal circles is found to be a good compromise between mechanical strength and achievable vibration amplitude. The thickness of the plate is 8.55 mm. A result of a Finite-Element calculation of the vibration mode at 20 kHz with two nodal circles is shown in Fig. 7.2. The analytical result from Equ. 6.3 is plotted together with the FEM result. The mode shape of both results agrees very well. After assembly, the resonant frequency of the entire system (transducer, horn, and plate) appears at about 19 kHz. An Adaptive Phase Locked Loop control algorithm (APLL) is used for tracking the resonant frequency of the system during operation (34).

7.1.2   Levitation force measurement

An experimental setup is built as shown in Fig. 7.3 to measure the levitation force produced by the presented disc levitation system. An aluminum plate with the same diameter as the radiation plate is positioned in opposite to the radiator. This sound-
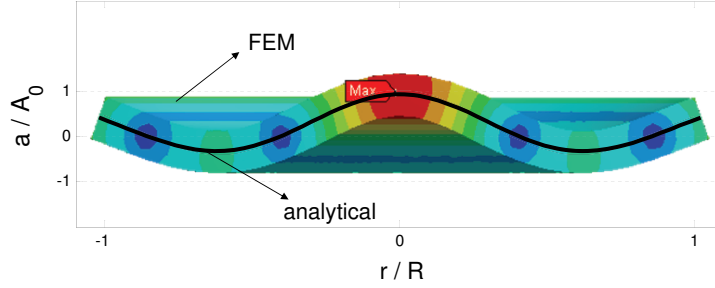
Figure 7.2: Calculation of the flexural vibration mode of the circular plate with two nodal circles (FEM and analytical results)

reflecting plate is mounted on a vertical linear stage through a load cell for being able to measure the vertical force acting on the reflector directly. Using the linear stage, the reflector may be positioned freely between the contact position and a distance of about 40 mm above the radiator. A laser interferometer is installed to measure the displacement of the reflector.

Measurements have been done with fixed voltage input of 50 V at a fixed frequency of 19 kHz (input power about 40 W). The actual vertical position of the reflector and the value of the levitation force are recorded simultaneously while the reflector slowly approaches the radiator from above until both plates get into contact. Levitation force versus distance between the plates is plotted in Fig. 7.4. Clear peaks of the levitation force can be seen in Fig. 7.4 at intervals of half wavelengths. The peak-values at the positions of half wavelengths increase with decreasing distance between the plates. The amplitude at the $\lambda/2$-position is about 1 N. Multiple peaks are observed near the positions of half wavelengths. This is because the nonlinear behavior of such a intensive sound beam. The uneven pressure distribution along the radial direction causes unequal sound speed. Therefore the standing wave is formed at slightly different positions for different parts of the sound beam.
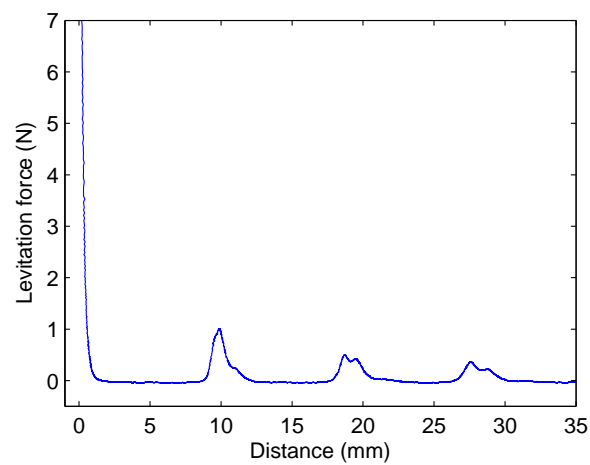
When the gap between the plates gets smaller than approximately 0.5 mm, the squeeze-film region is reached and the levitation force starts to increase significantly. A maximum levitation force up to 100 N is measured right before contact happens. The
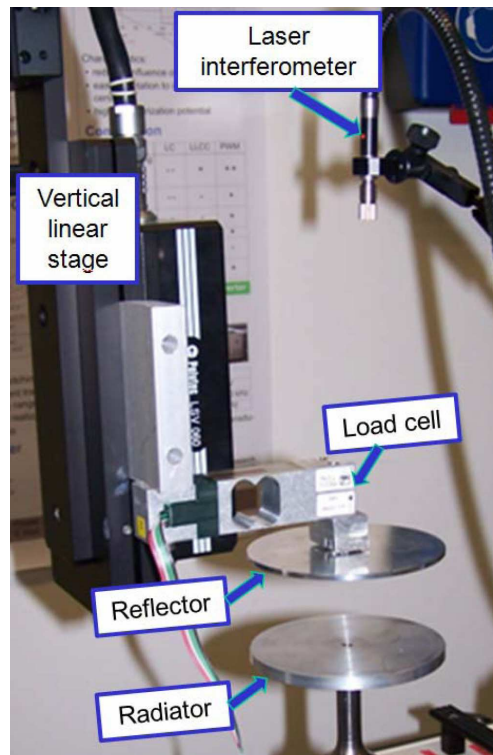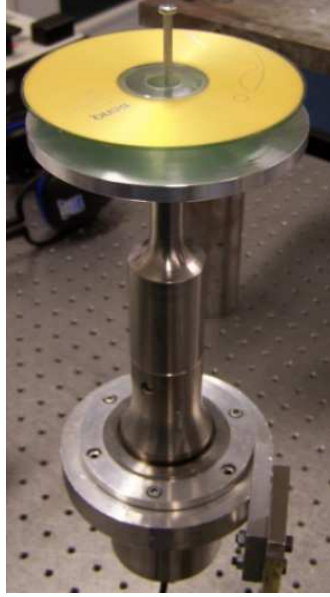
Figure 7.3: Experiment setup for measuring the acoustic radiation force

Figure 7.4: Levitation force versus levitation distance. Input power 50 W, frequency 19 KHz.

Figure 7.5: Stable levitation of a CD at half wavelength ($\lambda/2$) above the radiator. The central pin (screwed into the flexural plate) is used only for centering the plate in radial direction

squeeze film levitation effect will be discussed in Chap. 8.

7.1.3 Levitating a compact disc

A common compact disc (CD) is chosen as the object to be levitated. It has the same diameter as the vibrating plate, with a thickness of 1.3 mm and a mass of 16 g. A stable levitation state is observed when the input power reaches about 30 W (see Fig. 7.5). The CD then rests without any instable vertical motion above the flexural plate. Maximum vibration amplitude of the excitation system occurs at the center of the flexural plate and is about 25 μm at 19 kHz for this level of power (measured using a laser vibrometer). It is worth mentioning that the CD in this arrangement rests at a position slightly higher than half a wavelength (above the peak of the levitation force), where the levitation force equals the gravity force of the CD. This is different compared to common radiator-reflector-type systems, in which small particles are levitated at positions slightly below the pressure nodes of the standing wave. Stable levitation could not be achieved at one wavelength or higher positions with the proposed setup due to
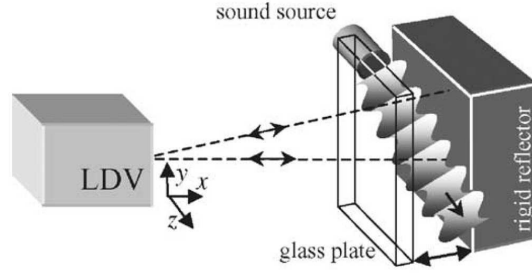
**Figure 7.6:** Interferometric measurement of a 2D sound field (68)

the quickly dropping levitation force.

7.1.4 Sound field visualization

Visualization of sound wave propagation and interaction with structures in the levitation mechanism is important for understanding the underlying acoustics. The conventional method to measure acoustic fields with microphones is difficult in the presented system, because the measuring volume is limited, high resolution is required, and disturbances due to sensors are not acceptable. Recently, Zipser et al. (68), (67) introduced a new method for planar visualization of acoustic sound waves in gases by means of a scanning laser vibrometer. The principle of interferometric measurement of a 2D sound field is shown in Fig. 7.6. The laser beam is projected though the sound field and reflected by the rigid reflector. The refractive index and the density of air chance with the pressure in the sound field. Therefore the optical length of laser also changes with the pressure. The optical length change is measured by the scanning laser vibrometer as if the rigid reflector has been moved. The measured movement can be re-modulated back to pressure change, so that the sound field is obtained. With this high sensitive method, multi-frequency, repetitive sound fields can be measured. This measurement technique is applied to study the sound field excited by the disc-shaped radiator and the interaction with the levitated objects. Since pictures of the qualitative distribution of pressure are sufficient here, no complicated post-processing is needed.

In the first experiment, the sound propagation from the vibrating radiator is visualized and shown in Fig. 7.7(a). Red color (darker color) indicates high pressure and
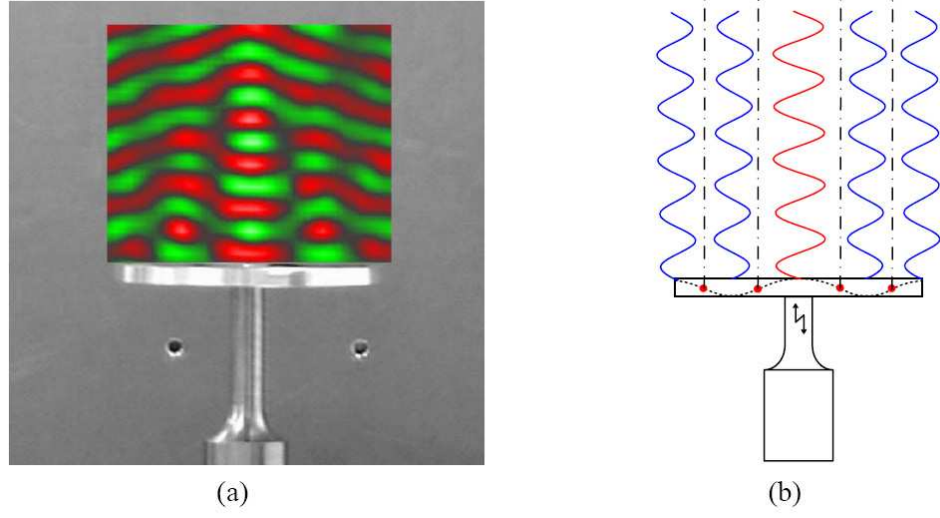
Figure 7.7: Sound wave free propagation above the radiator. a) measurement result; b) schematic diagram

green (brighter color) indicates low pressure; in an additional animated video the continuous propagation of the sound-wave has been visualized as schematically depicted in Fig. 7.7(b). Distinctive high and low pressure regions can be seen above the radiation surface within the first wavelength. Several interference patterns are observed starting from the second wavelength, which are typical for the acoustic near-field of this kind of radiators. The interfering regions coincide with the positions of the two nodal circles on the surface of the radiating plate as shown in Fig. 7.7(b).

Figure 7.8 shows the results measured when the CD is levitated and rests in a stable position slightly above half a wavelength. A clear standing wave pattern is seen in an animated depiction. Leak of sound pressure from the center hole of the CD is also observed. It can be stated that the levitated CD itself acts as a reflector for building the $\lambda/2$ standing wave between plate and the CD. The distinct high-low pressure distribution follows exactly the vibration mode of the radiator, which proves that the assumption made for the sound field model is acceptable.
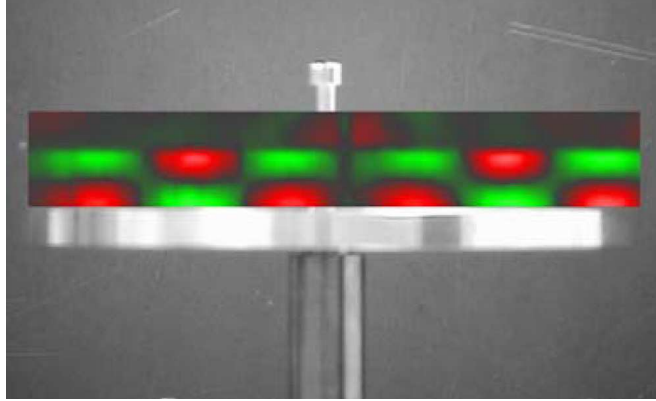
**Figure 7.8:** Visualization of the standing wave field during stable levitation, operating frequency 19 kHz

7.2 Results and discussion

The theoretical model to predict the radiation pressure has been established in Chap. 6. To use Equ. 6.15 to calculate the pressure, one needs first to know the acoustic pressure amplitude A_0. However, the acoustic pressure is difficult to measure in the presented arrangement due to the limited space. On the other hand, the mechanical vibration is much easier to obtain. The following arrangement is made to link the radiation pressure with the mechanical vibration of the radiation.

The magnitudes of air particle velocity $|\hat{v}_{r,z}|$ at each point according to r and z directions can be derived from Equ. 6.11 as

$$
\begin{aligned}
|\hat{v}_{r,z}| &= \frac{A_0 Z(r)}{\rho_0 c} \cdot \sqrt{(\cos kz \cdot \sinh \alpha' z)^2 + (\sin kz \cdot \cosh \alpha' z)^2} \\
&= \frac{A_0 Z(r)}{\rho_0 c} \cdot \sqrt{\sinh^2 \alpha' z + \sin^2 kz}
\end{aligned}
\tag{7.1}
$$

The distance from the reflector to the sound radiator is given as L. Therefor, $|\hat{v}_{0,L}|$ represent the air particle speed magnitudes directly on the center of the sound radiator, which can be found by setting $z = L$ and $r = 0$ in Equ. 7.1. Assuming that the air particles on the radiation surface move in the same way as the surface itself, $|\hat{v}_{0,L}|$ is equal to surface vibration speed amplitude at the center of the radiator, represented by V_0. Therefore, the acoustic pressure amplitude A_0 at $r = 0$ can be derived from Equ.
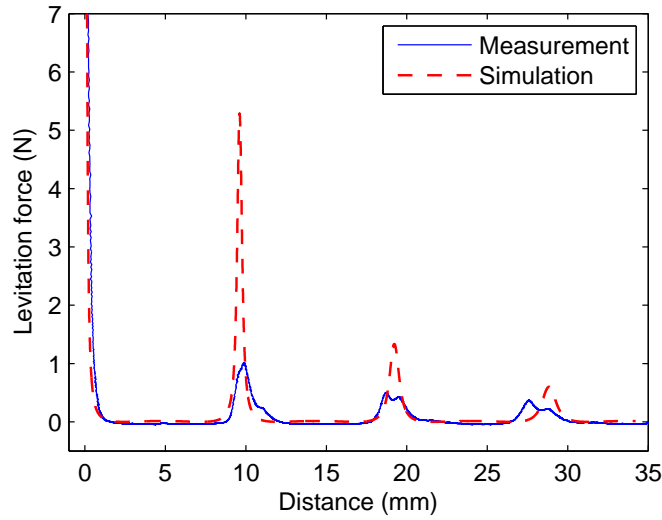
Figure 7.9: Levitation force versus levitation distance, experiment and calculation results

7.1 as

$$A_0 = V_0 \rho_0 c / \sqrt{\sinh^2 \alpha' L + \sin^2 kL} \tag{7.2}$$

Equ. 7.2 gives a relation between the mechanical vibration of the radiator and the acoustic field. It can be seen that for a given distance L and the surface vibration amplitude V_0 at $r = 0$, the acoustic pressure amplitude A_0 at $r = 0$ can be obtained. Substituting Equ. 7.2 into Equ. 6.15, we find

$$p_{ra} = Z(r)^2 \frac{V_0^2 \rho_0}{4 \left(\sinh^2 \alpha' L + \sin^2 kL \right)} \tag{7.3}$$

In Equ. 7.3, all the parameters except V_0 and α' are known for a given experiment setup. The vibration amplitude V_0 can be measured experimentally during operation. The increased absorption coefficient α' depends on α and the wave properties. The acoustic radiation pressure can be calculated using Equ. 6.8 and Equ. 7.3. The levitation force can then be obtained by integrating p_{ra} on the surface of the levitated object.

Results of calculated levitation forces for different L values are plotted in Fig. 7.9. The measured results are plotted together with the calculated ones. It can be seen that the calculated levitation forces agree well with the measurements. However, the magnitude at the position of half wavelength is about 5 time of the measured value.

The possible reasons of the higher calculated force are as following. First, the reflector used in the experiment is never a perfect reflecting surface. Diffraction and absorption always exist at the reflector. Secondly, in the experiment, the two plates are not perfectly parallel. Thus, the standing wave is not formed at one single distance, but in a small range. This has been proved by the multiple peaks measured in experiment discussed in Sec. 7.1. Therefore, the resulted levitation force is more distributed with smaller amplitude compared to the simulation.

7.3   Conclusion

Experimental investigation on a non-contact suspension system for large planar objects has been presented in this chapter. A CD is successfully levitated with the proposed system at a height of half a wavelength. The levitation forces at different distances have been measured. A force of about 1 N has been observed at the position of half wavelength in front of the sound radiator.

The presented non-contact suspension system can be used for non-contact handling of sensitive parts such as a silicon wafer. With the high levitation distance, the levitated part can be processed on both sides without additional contact. The proposed system can be also used as a non-contact thrust bearing when the load-capacity is not the primary concern for the bearing. Another possible application is to use the system as a non-contact actuator to give a certain actuation force on a planar surface from a certain distance without mechanical contact.

8

Squeeze film ultrasonic levitation

The working principles of squeeze film levitation will be explained in this chapter. As before, analytical models will be discussed first, since they provide insight to the parameters that are crucial to the performance of a squeeze film levitation system. Two analytical models based on acoustic theory and fluid dynamics will be presented and compared. After that, the governing fluid dynamics equation is solved numerically to obtain more precise results.

8.1 Modeling based on acoustic theory - acoustic radiation pressure

Squeeze film levitation happens when a planar object is brought close to an oscillating surface which vibrates at high frequency (often in ultrasonic range). The object will experience a normal pressure and can be levitated above the vibrating surface at a very small distance (normally a few to several tens μm). Unlike the levitation system introduced in Chap. 6, the standing wave field does not exist anymore in squeeze film levitation. Instead, a very thin air film with pressure varying according to the movement of the radiation surface is to be considered. The physical model shown in Fig. 2.2 is considered. Since the vibration of the plate in squeeze film levitation is piston-like, the wave is considered as a plane wave. Moreover, the distance h_0 between two surfaces is normally of order 10^{-5} m, which is three orders smaller than the dimension of the vibrating surface L (with order of 10^{-2} m). Thus the lateral movement of the air is

8. SQUEEZE FILM ULTRASONIC LEVITATION

neglected, resulting in a closed boundary plane wave, which can be described as

$$p = A_0 \, \cos(\omega t - kz) \tag{8.1}$$

where A_0 is the amplitude of acoustic pressure, k the wave number, ω the angular velocity of the wave and z the distance from the vibration source. With the above assumptions, the system can be considered as an extreme case of the disc levitation system discussed in Chap. 6 when the object (reflector) is brought very close to the radiator. Therefore it can be described in the same manner using the model of the disc levitation system. Since the traveling distance of the wave in squeeze film levitation is very small, the absorption effect can be neglected safely. Considering the multiple reflection of the waves between two rigid surfaces, the resulting sound field can be described similarly as Equ. 6.10 as

$$p = A_0 \, \cos kz \, \cos \omega t \tag{8.2}$$

The corresponding acoustic velocity v in z direction is derived as

$$v = \frac{A_0}{\rho_0 c} \, \sin kz \, \cos(\omega t - \pi/2) \tag{8.3}$$

Similar as the procedure in Sec 6.2.4, according to Equ. 4.12 and 4.13, $\langle V \rangle$ and $\langle K \rangle$ can be derived using Equ. 8.2 and Equ. 8.3 as

$$\langle V \rangle = \langle p^2 \rangle / 2\rho_0 c^2 = \frac{A_0^2}{4\rho_0 c^2} \, \cos^2 kz \tag{8.4}$$

$$\langle K \rangle = \rho_0 \langle v \cdot v \rangle / 2 = \frac{A_0^2}{4\rho_0 c^2} \, \sin^2 kz \tag{8.5}$$

Substituting Equ. 8.4 to 8.5 into Equ. 4.32, the mean Eulerian excess pressure is obtained as

$$p_{\mathrm{ra}} = \langle V \rangle - \langle K \rangle + C = \frac{A_0^2}{4\rho_0 c^2} \cos 2kz + C = E \cos 2kz + C \tag{8.6}$$

where E is the energy density of the considered wave. For a closed plane wave sound field, constant C is derived from the conservation of mass as (30)

$$C = \frac{\Gamma - 1}{2} E \tag{8.7}$$

Therefore, we have

$$p_{\mathrm{ra}} = \left(\frac{\Gamma - 1}{2} + \cos 2kz \right) E \tag{8.8}$$

where Γ is a specific heat ratio, $\Gamma = 1.4$ for air. To calculated the radiation pressure using Equ. 8.8, one needs first to know the acoustic pressure amplitude A_0. Similar as Equ. 7.2, the acoustic pressure amplitude A_0 can be expressed in terms of the vibration velocity amplitude V_0 as

$$A_0 = V_0 \rho_0 c / \sin k h_0 \tag{8.9}$$

In which h_0 is the mean distance between the two plane surfaces. Substituting Equ. 8.9 in to Equ. 8.8, we find

$$p_{\mathrm{ra}} = \left(\frac{\Gamma - 1}{2} + \cos 2kz \right) \frac{V_0^2 \rho_0}{4 \sin^2 k h_0} \tag{8.10}$$

Since z and and h_0 are in the order of 10^{-4} m and k is in the order of 10^2, kz and $k h_0$ are in the order of 10^{-2}, the relations $\sin k h_0 \approx k h_0$ and $\cos 2kz \approx 1$ hold. Given $a_0 = V_0 / \omega$ as the oscillating displacement amplitude, Equ. 8.10 can be then simplified as

$$p_{\mathrm{ra}} = \frac{\Gamma + 1}{8} \frac{V_0^2 \rho_0}{k^2 h_0^2} = \frac{\Gamma + 1}{8} \frac{a_0^2 \rho_0 c^2}{h_0^2} \tag{8.11}$$

It can be seen that the radiation pressure p_{ra} in squeeze film levitation is reversely proportional to the square of the levitation distance and proportional to the square of the vibration displacement amplitude a_0. The levitation force can be then obtained by integrating p_{ra} along the levitated object. The physical boundary condition of Equ. 8.11 is $a_0 < h_0$ to avoid contact. Therefore, p_{ra} reaches its theoretical maximum when $a_0 = h_0$.

For an oscillating surface with uneven but known vibration amplitude distribution, the squeeze levitation force can still be calculated using Equ. 8.11 by considering the uneven vibration as a sum of finite number of small piston-like vibrations. Since the lateral movement of the gas is neglected, the small piston vibrators can be treated individually and the resulting mean levitation pressure is the average of the levitation forces induced by all the small piston vibrators. Taking the flexural circular plate radiator presented in Chap. 6 as an example, the governing equation of surface amplitude distribution is $Z(r)$ as presented in Sec. 6.2.1. The mean squeeze film levitation pressure induced by the flexural vibration mode can be calculated as

$$p_{\mathrm{mean}} = \frac{1}{R} \int_0^R \frac{\Gamma + 1}{8} \frac{(A_0 Z(r))^2 \rho_0 c^2}{h_0^2} \mathrm{d}r = \frac{\Gamma + 1}{8} \frac{A_0^2 \rho_0 c^2}{h_0^2} \int_0^R Z(r)^2 \mathrm{d}r \tag{8.12}$$

where R is the radius of the circular radiator, r the radial position on the radiator, A_0 the maximum vibration amplitude at the center of the radiator.

8.2 Modeling based on fluid mechanics - solving the Reynolds equation

A sound wave is an oscillation of pressure. In squeeze film levitation, the wavelength of the sound wave that would be generated by the oscillating surface is several orders larger than the gap distance. Assuming that a sound wave is propagating in such a small distance, the pressure gradient in the direction of propagation (normal to the surface) will be extremely small. If the pressure gradient is small enough to be ignored, the assumption of sound propagation does not hold anymore. In such a case, an acoustic radiation pressure based on the propagation of sound wave seems not reflecting the actual physical condition of squeeze film levitation. Alternatively, a model based on fluid dynamics which considers the viscous lateral flow of gas in a narrow gap may give a better insight to the physical condition and provide better simulation results for the highly squeezed gas film.

The differential equation governing the pressure distribution of a fluid film between two opposing surfaces is called Reynolds Equation. This equation was first derived in a remarkable paper by Osborne Reynolds in 1886. The Reynolds Equation can be derived from the Navier-Stokes equation and continuity equation or directly from the principle of mass conservation. The detailed derivation of Reynolds Equation can be found in literatures such as (18), therefore the general form of Reynolds Equation is given directly here.

$$\frac{\partial}{\partial x}\left(\frac{\rho h^3}{12\eta}\frac{\partial p}{\partial x}\right)+\frac{\partial}{\partial y}\left(\frac{\rho h^3}{12\eta}\frac{\partial p}{\partial y}\right) = \frac{\partial}{\partial x}\left[\frac{\rho h(u_a+u_b)}{2}\right]+\frac{\partial}{\partial y}\left[\frac{\rho h(v_a+v_b)}{2}\right]+\frac{\partial(\rho h)}{\partial t} \quad (8.13)$$

where, ρ represents the density of the fluid, h the gap distance, p the pressure, η the absolute viscosity, t the time, u and v the velocity in x and y directions with subscription a and b denoting the upper and lower limits of the fluid film.

Considering the Reynolds equation valid for squeeze film levitation shown in Fig.2.2, u_a, u_b and v_a, v_b are zero since the surfaces have no lateral movement. Equation 8.13

can be simplified as

$$\frac{\partial}{\partial x}\left(\frac{\rho h^3}{12\eta}\frac{\partial p}{\partial x}\right) + \frac{\partial}{\partial y}\left(\frac{\rho h^3}{12\eta}\frac{\partial p}{\partial y}\right) = \frac{\partial(\rho h)}{\partial t} \qquad (8.14)$$

The equation of state for a perfect gas is

$$p = \rho \bar{R} t_m \qquad (8.15)$$

where $\bar{R}$ represents the gas constant and t_m the absolute temperature. Therefore we have

$$\rho = \frac{p}{\bar{R} t_m} \qquad (8.16)$$

Substituting this equation in to Equ. 8.14 yields

$$\frac{\partial}{\partial x}\left(\frac{p h^3}{12\eta}\frac{\partial p}{\partial x}\right) + \frac{\partial}{\partial y}\left(\frac{p h^3}{12\eta}\frac{\partial p}{\partial y}\right) = \frac{\partial(p h)}{\partial t} \qquad (8.17)$$

In practice, it is often sufficient to consider the 1-D case of Equ. 8.17, which can be written as

$$\frac{\partial}{\partial x}\left(\frac{p h^3}{12\eta}\frac{\partial p}{\partial x}\right) = \frac{\partial(p h)}{\partial t} \qquad (8.18)$$

The following dimensionless parameters are defined,

$$P = \frac{p}{p_0}, \ H = \frac{h}{h_0}, \ X = \frac{x}{L}, \ T = \omega t, \ \sigma = \frac{12\omega\eta L^2}{p_0 h_0^2}$$

where σ is named squeeze number, L the characteristic length of the gas film. Substituting above dimensionless parameters in the Equ. 8.18, we obtain (18)

$$\frac{\partial}{\partial X}\left(PH^3\frac{\partial P}{\partial X}\right) = \sigma\frac{\partial(PH)}{\partial T} \qquad (8.19)$$

Equ. 8.19 is the second order partial differential equation that governs the time-dependent, laminar, Newtonian, isothermal and compressible thin film flow.

In general, Equ. 8.19 can not be solved analytically except for some special cases (38; 47; 61). It has to be solved numerically for the distribution of pressure P along X and Y (23; 37; 39; 51). The analytical and numerical solutions of Reynolds equitation will be discussed in the following sections.

8.2.1 Approximate solution of the Reynolds equation for large squeeze number

For the case illustrated in Fig. 2.2, a flat surface oscillates in the normal direction against a fixed flat wall parallel to it. At high squeeze number, the gap thickness become much smaller than the length, the volume flow at the peripheries becomes very small. Thus the system can be considered as a gas film in a closed channel being compressed at one side and closed at the other. By assuming isothermal condition, the mass conservation yields

$$PH = \Psi \tag{8.20}$$

where Ψ is a constant. Equation 8.19 can be rewritten as

$$\frac{\partial}{\partial X}\left(\Psi H^2 \frac{\partial(\Psi/H)}{\partial X}\right) = \frac{\partial}{\partial X}\left(\frac{1}{2}H\frac{\partial(\Psi^2)}{\partial X} - \Psi^2\frac{\partial H}{\partial X}\right) = \sigma\frac{\partial(\Psi)}{\partial T} \tag{8.21}$$

Since the gap is assumed as independent from length X, we have $\partial H/\partial X = 0$. The above equation becomes

$$\frac{\partial}{\partial X}\left(\frac{1}{2}H\frac{\partial(\Psi^2)}{\partial X}\right) = \sigma\frac{\partial(\Psi)}{\partial T} \tag{8.22}$$

Under the above assumptions, by integrating both sides of Equ. 8.22 over a time period yields (47)

$$\int_0^{2\pi}\frac{\partial}{\partial X}\left(\frac{1}{2}H\frac{\partial(\Psi^2)}{\partial X}\right)\,\mathrm{d}T = \sigma\int_0^{2\pi}\frac{\partial(\Psi)}{\partial T}\,\mathrm{d}T = 0 \tag{8.23}$$

Integrating Equ. 8.23 with respect to X yields

$$\int_0^{2\pi}H\frac{\partial(\Psi^2)}{\partial X}\,\mathrm{d}T = C_1 \tag{8.24}$$

Equ. 8.24 holds for all values of X. Since the system is symmetric, the pressure gradient at the center of the gap should satisfy the condition $\partial P/\partial X = 0$. Therefore, at $X = 0$, the left hand side of Equ. 8.24 is equal to zero. In turn, C_1 is equal to 0 also. By integrating Equ. 8.24 with respect to X again, we obtain

$$\int_0^{2\pi}H\Psi^2\,\mathrm{d}T = \int_0^{2\pi}H^3P^2\,\mathrm{d}T = C_2 \tag{8.25}$$

C_2 can be found be applying the boundary condition of $P = 1$ at the peripheries of the gap and setting $H = 1 + \epsilon\sin T$ as

$$C_2 = \int_0^{2\pi}H^3\,\mathrm{d}T = \int_0^{2\pi}(1 + \epsilon\sin T)^3\,\mathrm{d}T = \pi(2 + 3\epsilon^2) \tag{8.26}$$

Substituting Equ. 8.26 and $H = 1 + \epsilon \sin T$ into Equ. 8.25 yields

$$\int_0^{2\pi} H\Psi^2 \, \mathrm{d}T = \Psi^2 \int_0^{2\pi} (1 + \epsilon \sin T) \, \mathrm{d}T = \pi(2 + 3\epsilon^2) \tag{8.27}$$

Ψ is found readily as $\Psi = \sqrt{1 + 3/2\epsilon^2}$, and we obtain P as

$$P = \frac{\Psi}{H} = \frac{\sqrt{1 + \frac{3}{2}\epsilon^2}}{1 + \epsilon \sin T} \tag{8.28}$$

The time and space averaged mean pressure in the gap can then be obtained as

$$\bar{P} = \frac{1}{2\pi} \int_0^{2\pi} P \, \mathrm{d}T = \frac{1}{2\pi} \int_0^{2\pi} \frac{\sqrt{1 + \frac{3}{2}\epsilon^2}}{1 + \epsilon \sin T} \, \mathrm{d}T = \sqrt{\frac{1 + \frac{3}{2}\epsilon^2}{1 - \epsilon^2}} \tag{8.29}$$

This approximate solution based on mass conservation gives a mean pressure along the entire length of the gap and is independent of the squeeze number. It is suitable only for conditions with high squeeze number (47).

8.2.2 Solving the Reynolds equation numerically

In order to obtain the pressure distribution along the gap, Equ. 8.19 is solved numerically using the finite difference method. Since the considered problem is symmetric in X, only one half of the length L (from the center $X = 0$ to $X = 1/2$) is considered in the calculation to reduce the computation cost. By applying a finite difference scheme in X, one half of the length is divided into N finite lengths ΔX. Equation 8.19 then takes the form of a set of ordinary normalized differential equations in time

$$\sigma \frac{\mathrm{d}P_i(T)}{\mathrm{d}T} = -\sigma \frac{P_i(T)}{H} \frac{\mathrm{d}H}{\mathrm{d}T} + \frac{H^2}{X_i} \frac{1}{2\Delta X^2}$$
$$\left[X_{i+\frac{1}{2}} \left(P_{i+1}^2 - P_i^2 \right) - X_{i-\frac{1}{2}} \left(P_i^2 - P_{i-1}^2 \right) \right] \tag{8.30}$$

The subscript i indicates the grid coordinate along the x axis. The initial pressure in the gap at $T = 0$ is assumed to be equal to the ambient pressure p_0. The boundary condition at the edge of the plate is set as pressure release which means that the pressure near the edge always approaches to p_0. At the center of the plate ($X = 0$) there should be no pressure gradient along the x-direction, so that the pressure gradient across the complete gap is always differentiable and no local extreme exists. This means $P_0 = P_1$

at all time points. To sum up, the initial condition and boundary conditions are listed as following:

$$\text{Initial condition: } P(X, T = 0) = 1$$
$$\text{Boundary condition 1: } P(X = 1/2, T) = 1$$
$$\text{Boundary condition 2: } \frac{\partial P(X = 0, T)}{\partial X} = 0$$

Equ. 8.30 can be solved easily with mathematical tool such as MATLAB.

8.3 Results and discussion

By numerically solving Equ. 8.30, the pressure distribution along half of the gap length can be obtained as a function of time. For a typical levitation system with $L = 30$ mm, $a_0 = 5$ μm, $f = 20$ kHz, pressure distribution for three different gap distances of 10 μm, 50 μm and 100 μm are calculated and shown in Fig. 8.1. The corresponding squeeze numbers are 2425, 97 and 24 respectively. It can be seen that the pressure in the gap oscillates with time according to the movement of the vibrating surface. The peak values are higher than the absolute anti-peak values, which leads to a positive time-averaged pressure. As specified in the boundary condition 1, the pressure at the edge of the plate is always equal to atmosphere pressure. The pressure increases as moving inside the gap. For high squeeze number (Fig. 8.1 (a)) the pressure increases quickly to maximum and keeps constant along the length; for small squeeze number (Fig. 8.1 (c)), the pressure increases gradually and reaches maximum at the center.

8.3.1 Experimental validation

In order to examine the accuracy of the calculation results from the models presented above, a series of experiments are conducted and compared with the simulation results.

The squeeze film levitation force is measured with the same setting as when measuring the acoustic radiation force. Fast increasing of levitation force has been measured when the levitation distance gets smaller than 0.5 mm. A maximum levitation force of 28 N is obtained with input power of 50 W at frequency of 19 kHz. The mean levitation distance h is 63 μm before some regions get into contact. The diameter of the circular

(a) σ = 2425, ε = 0.5

(b) σ = 97, ε = 0.1

(c) σ = 24, ε = 0.05
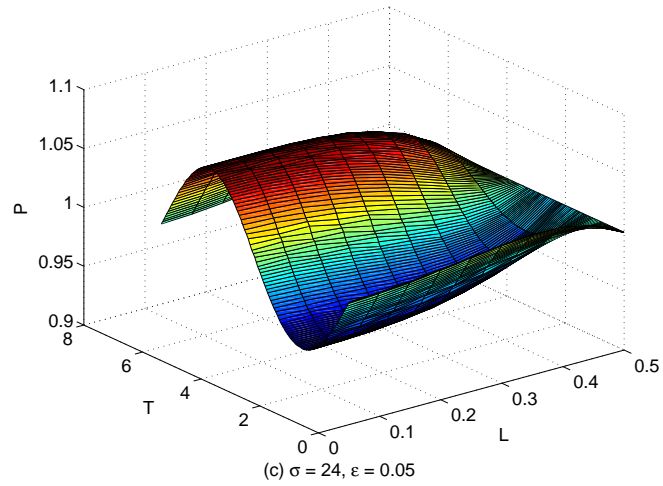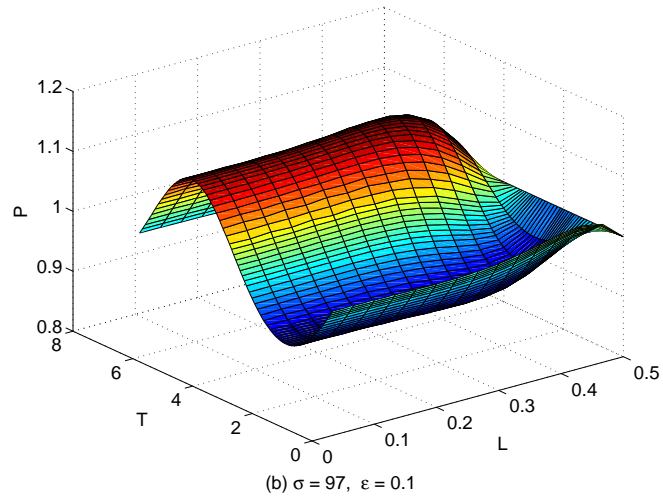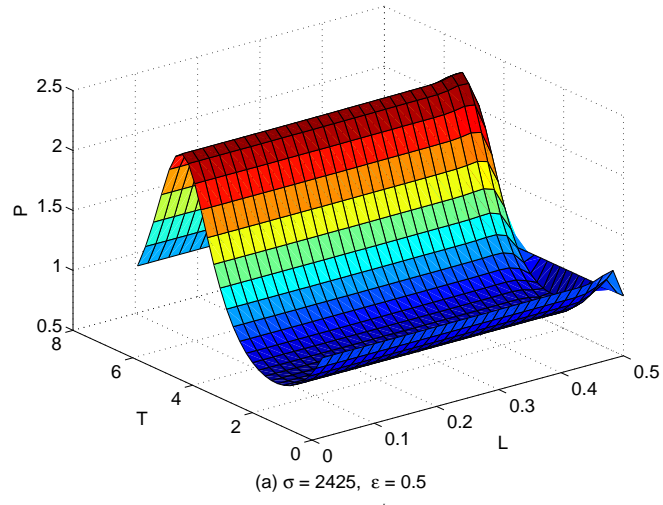
Figure 8.1: Numerical simulation results for the pressure distribution along the gap varying with time
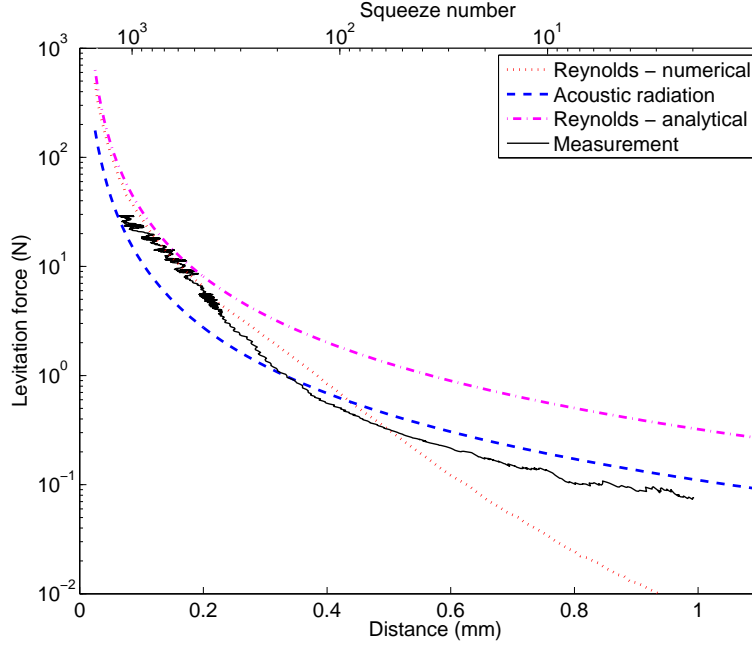
Figure 8.2: Comparison of the measured and calculated levitation forces

radiator is 120 mm with vibration amplitude 40 μm at the center. The vibration amplitude distribution is shown in Fig. 6.2. Actual parameters of the presented levitation system are used to calculate the pressure. The mean vibration amplitude along the surface is 15 μm which is used for the simulation. The gap distance is varied to mimic the situation when measuring the levitation force in the experiment. The squeeze film levitation force is plotted in Fig. 8.2 together with calculation results obtain from the acoustic radiation model (Equ. 8.12), the approximated (Equ. 8.29) and the numerical (Equ. 8.30) solution of the general Reynolds equation. For the analytical solution of Reynolds equation and the acoustic radiation pressure, the calculated mean pressure is multiplied by the area of the radiator to get the mean levitation force. The distributed pressure obtained from the numerical solution of Reynolds equation is integrated over the surface to get the mean levitation force.

It can be seen that all models give the correct tendency for the levitation force with respect to the levitation distance. At large distance (squeeze number<100) the measured curve agrees well with the calculated result from the acoustic radiation model.

The numerical result of Reynolds equation is much lower than the measurement. When the gap distance gets smaller (higher squeeze number), the measured pressure increased faster than the acoustic radiation model, and fits better to the numerical and analytical results of Reynolds equation. The transition happens at the position with squeeze number of about 100. The approximated solution of the Reynolds equation agrees with the numerical solution well at high squeeze number, but is much higher in case of low squeeze number. The different fitting of the curves at different levitation distance ranges can be explained as following. In the 1-D model based on acoustic theory, the gas is considered as inviscid and has no lateral movement. The wave is considered as propagating and bouncing within a very small distance between two surfaces. These assumptions are suitable when the gap distance h_0 is still comparable with the sound wavelength λ (i.e. $h_0/\lambda > 10^{-2}$) and the vibration amplitude a_0 is small compared to h_0. When the gap distance become more than two orders smaller than the sound wavelength and length of the gap L (resulting a high squeeze number), the squeeze effect becomes dominant. At the edge of the gap, the gas will be squeezed out and sucked in according to the oscillation of the surface. In the interior region, the gas does not have enough time to be squeezed out in the short time cycle. Therefore, the gas is just being pressurized and released according to the movement of the oscillating surface. Such a physical condition is exactly what the Reynolds equation represents for, therefore, as expected and observed in the Fig. 8.2, the fluid dynamic model fits better to the experiment result at higher squeeze number.

In order to have a close look on the squeeze film levitation force, a modified experimental setup is constructed as shown in Fig. 8.3. Instead of the flexural plate radiator, a $\lambda/2$ aluminum cylinder with diameter of 50 mm is used to provide a piston-like vibration. A plate is mounted on a force sensor through a ball joint to keep it parallel to the vibrating surface during the measurement. The measurement is conducted with a vibration amplitude of 10 μm on the surface at a frequency of 20 kHz. The gap distance is slowly reduced from 300 μm by adjusting the vertical stage until the two surfaces get into contact. A maximum levitation force of 115 N is measured at input power of about 50 W. Similar as for Fig. 8.2, the measured force is plotted in Fig. 8.4 together with the theoretical calculation results.
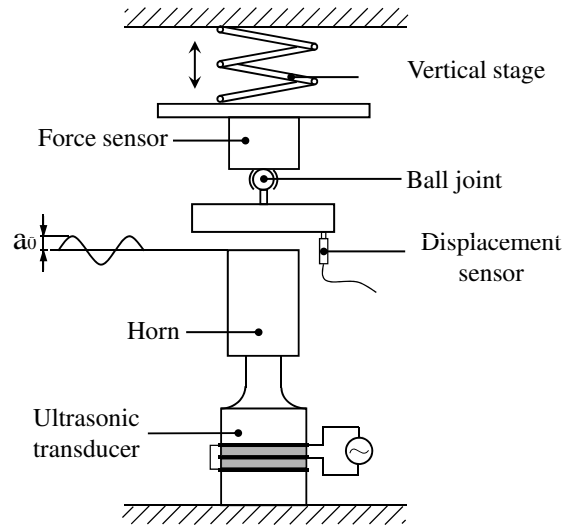
Figure 8.3: Experiment setup for measuring squeeze film levitation force
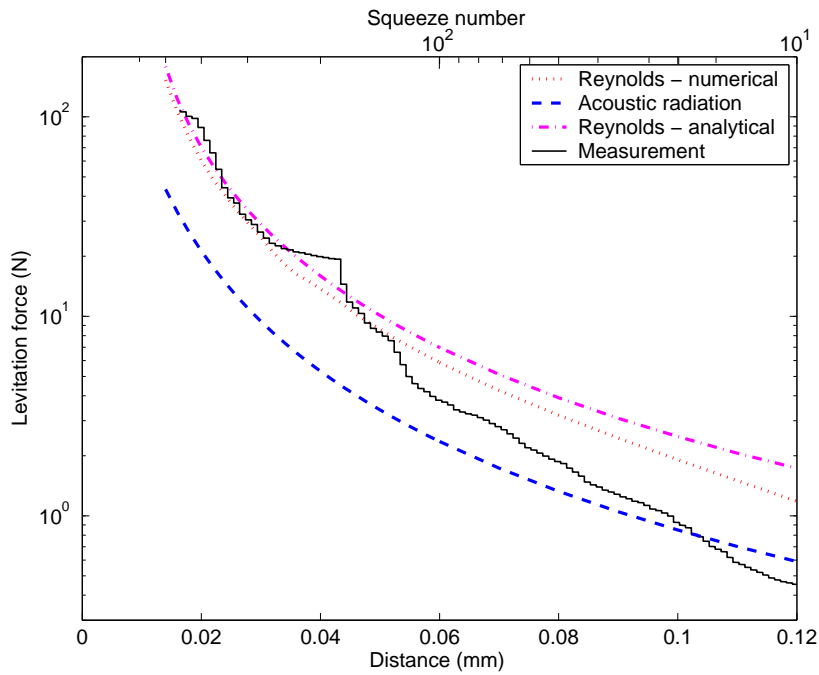

Figure 8.4: Comparison of the measured and calculated levitation forces

As expected, the measurement results agree well with the solution of Reynolds equation for the squeeze number higher than 100. At squeeze number lower than 100, the measured result is closer to the calculated force from acoustic radiation pressure.

It can be concluded that for a squeeze film levitation system with high squeeze numbers (> 100), the levitation force can be predicted precisely using the Reynolds equation. For very high squeeze numbers (> 1000), the approximated analytical solution of Reynolds equation can be applied instead of solving it numerically, since they agree to each other very well at this level of squeeze number. For the systems with low squeeze numbers (< 100), the acoustic radiation pressure model gives rather accurate results for predicting the levitation force.

8.3.2 Crucial parameters

For a squeeze film levitation system, a high levitation capacity (force per unit area) is always desirable. Therefore it is important to investigate how the various parameters affect the levitation capacity. Based on the simulation and experimental results, two parameters are found to have great influence on the load capacity of a squeeze film levitation system which are the squeeze number, σ and the excursion ratio, ϵ. The significance of σ and ϵ will be discussed in the following of this section.

- Squeeze number σ

If one takes a close look at the definition of the squeeze number ($\sigma = 12\omega\eta L^2/p_0 h_0^2$), it is easy to find that the squeeze number actually indicates how "intensive" the squeeze action is. It contains three important parameters, namely the driving frequency ω, the gap length L and the gap distance h_0. When other parameters of a levitation system are fixed, to increase the squeeze number, ω or L/h_0 can be increased. A higher ω means a faster squeeze motion. If the amplitude is kept unchanged, higher ω means more energy is brought into the gap. The ratio between L and h_0 indicates how big the levitation surface relatively is. Fig. 8.5 shows the numerical calculation results of pressure distribution in the gas film at different squeeze numbers. It can be seen from Fig. 8.5 that at a lower squeeze number, the pressure increases slowly from the edge of
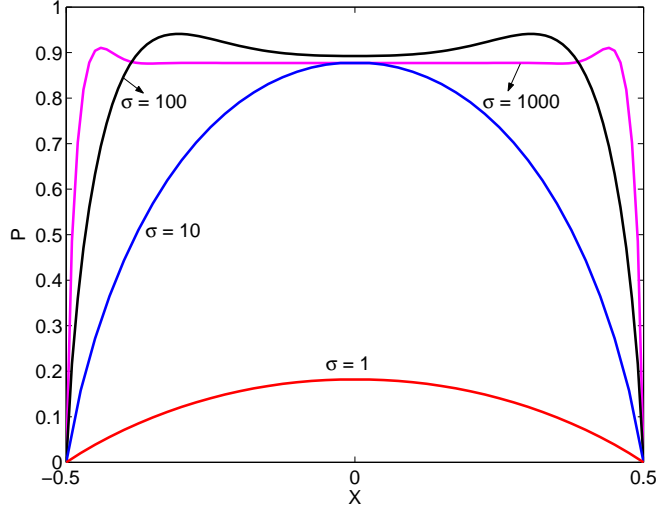
Figure 8.5: Numerical result of mean pressure distribution in the gap at different squeeze numbers

the gap and reaches peak at the center. When the squeeze number gets higher, the pressure increases quickly to maximum and distribute more evenly along the gap. Further increase of squeeze number does not help much to obtain higher levitation pressure any more. Therefore, when designing a squeeze film levitation system, a minimum squeeze number higher than 100 is necessary for building up the pressure efficiently.

As Salbu (47) concluded, the squeezed air film behaves as if it is incompressible at the boundary and solely compressible in the interior. The interior area increases from zero to the full length of the wall, while increasing the squeeze number. The interior region behaves like a spring with pressure in phase with vibration displacement. The exterior region behaves like a damper with pressure in phase with the vibration velocity.

- Excursion ratio ϵ

It is clearly seen from Fig. 8.2 and 8.4 that the levitation pressure increases with reducing the gap distance while the vibration amplitude is kept constant. Such a relation can be seen from Equ. 8.28 and 8.11 that the levitation force is roughly proportional to the square of the excursion ratio ϵ.
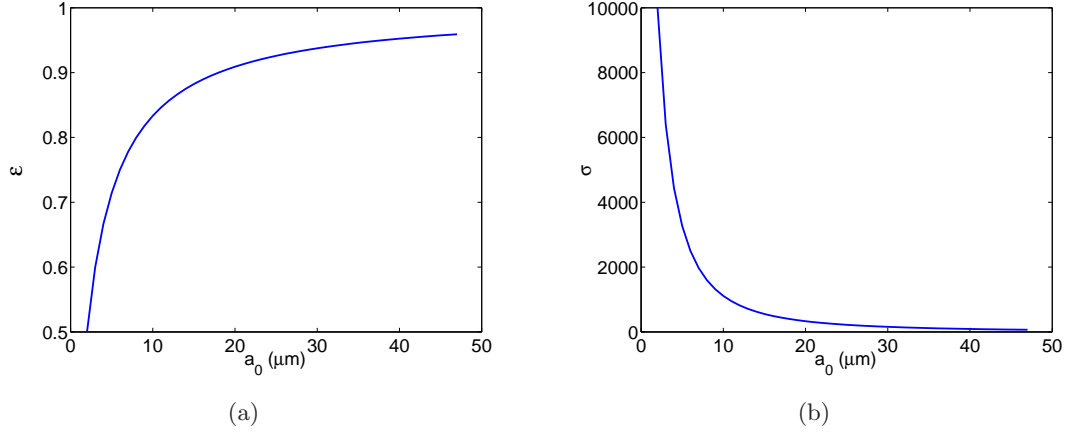
Figure 8.6: Change of (a), excursion ration ϵ and (b), squeeze number σ with respect to the vibration amplitude a_0. $\delta = h_0 - a_0 = 2\ \mu$m
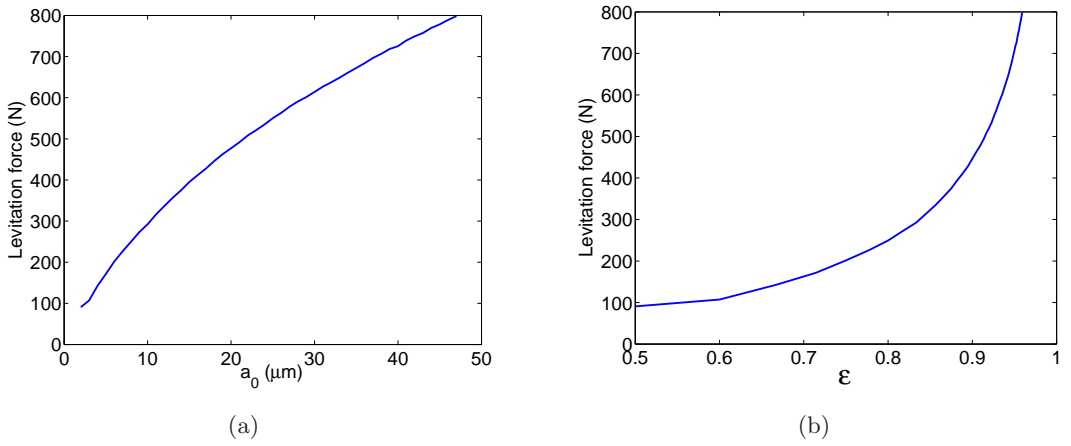
Figure 8.7: Change of levitation force with respect to (a), vibration amplitude a_0 and (b),excursion ration ϵ. $\delta = h_0 - a_0 = 2\ \mu$m

The levitation capacity of the system shown in Fig. 8.3 at different ϵ values is calculated to demonstrate the influence of ϵ and a_0. In the simulation, the vibration amplitude a_0 is varied, while the gap distance h_0 is kept as always 2 μm higher than a_0. The excursion ratio and squeeze number are determined according to the given vibration amplitude values (as shown in Fig. 8.6). The levitation capacity is calculated from the numerical solution of Reynolds equation and plotted with respect to ϵ and a_0 in Fig. 8.7. It can be seen that the levitation capacity increases with higher excursion ratio. The levitation capacity approaches infinite when the excursion ratio approaches one.

From the definition of the excursion ratio, we can see $\epsilon = 1$ if $a_0 = h_0$. In reality $a_0 = h_0$ means that at the highest position of the oscillation, the gap between the two surfaces is zero. Such a situation is impossible to achieve in practice since there will be always a small mean gap δ ($\delta = h_0 - a_0$) between two surfaces due to the surface roughness and flatness error as well as the misalignment between two surfaces. The excursion ratio ϵ is then $a_0/(\delta + a_0)$. The minimum gap δ is usually a constant finite value for a certain system. For example, in the experiment shown in Fig. 8.3, contact happens at a mean gap distance of 23 μm and vibration amplitude of 10 μm ($\epsilon = 0.45$ and $\delta = 13$ μm). In practice, ϵ can only approach one if δ approaches zero or a_0 is much larger than δ. The minimum gap δ can be reduced only by higher manufacturing accuracy. Higher a_0 can be achieved by proper design of ultrasonic transducers.

In conclusion, for a squeeze film levitation system, a sufficiently high squeeze number ($\sigma > 100$) is essential to build up the pressure efficiently in the gap. This has to be considered during the design phase. The maximum achievable levitation capacity of a squeeze film levitation system is determined by the excursion ratio ϵ. The excursion ratio ϵ depends on the vibration amplitude a_0 and δ. The mean gap δ always exists and is constant for a specific system. It can only be minimized by better manufacturing accuracy. Therefore, good surface finishing and form accuracy are important for a squeeze film levitation system to achieve higher levitation capacity. A higher vibration amplitude is helpful to achieve higher levitation capacity when δ can not be further reduced. In other words, a higher a_0 makes the system performance less sensitive to δ.
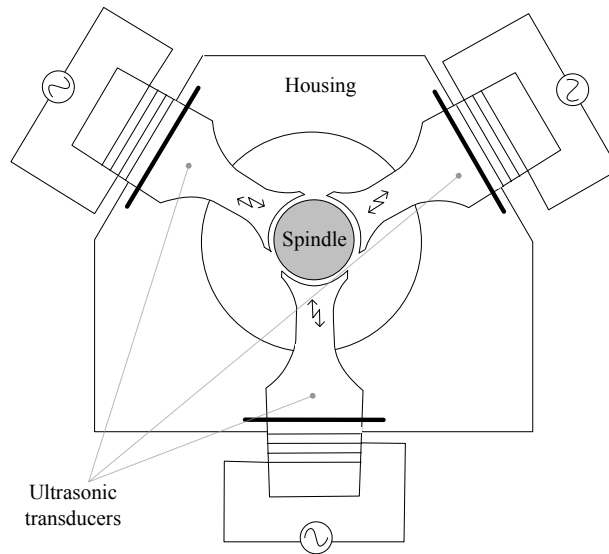
9

An non-contact journal bearing based on squeeze film ultrasonic levitation

According to the discussion in Chap. 8, squeeze film levitation can provide considerably high load-carrying capacity (levitation force per unit area) by properly designing the system. It is suitable to be applied to develop non-contact suspension systems. As discussed in Sec. 2.2.2, several linear bearings based on squeeze film levitation have been developed with satisfactory performance. Rotational bearings have been rarely investigated due to the non-flat surfaces and the requirement of multiple directional supports. The existing squeeze film rotational bearings uses either bulk piezoelectric materials (14; 56) or flexural vibration mode of piezoelectric elements or flexural hinges (51; 61; 66). They all suffer from very limited load capacity and are not suitable for high-load applications.

In this chapter, an improved design of a non-contact squeeze film journal bearing using Langevin ultrasonic transducers will be presented. The proposed bearing has a much higher load capacity and is aimed for applications such as bearing for precision machine tool spindle systems. The design and experimental results will be discussed in this chapter.

Figure 9.1: Schematic diagram of the proposed bearing system

9.1 Design of the proposed bearing

The proposed bearing consists of three piezoelectric transducers mounted on a housing, in a circle with 120 degree between each other. The center lines of all the transducers go through the rotation center of the spindle. A schematic diagram is shown in Fig. 9.1. Each transducer has a concave radiation surface which covers about 100 degrees of a cylindrical surface. The three radiation surfaces form the bearing inner ring, which has a diameter slightly larger than the spindle. When the transducers are driven to vibrate in their first longitudinal resonance, squeeze film levitation effect takes place between the inner bearing ring and the spindle surface. Repelling force is generated in the air gap which suspends the spindle and automatically keeps it at the equilibrium position. Active control of the transducers is not necessary, since the bearing is naturally a stable system. However, the actual position of the spindle center is monitored precisely during operation by two inductive sensors, which allows a detailed investigation of the system's behavior. And, of course, by controlling the three transducers in an appropriate way, an active bearing can be realized.

9.1.1 The Langevin ultrasonic transducer

The piezoelectric transducers are the key parts for the ultrasonic bearing system. They generate high frequency mechanical vibration for creating strong and stable squeeze film levitation. The basic working principles and design methods of piezoelectric transducers have been discussed in Chap. 5. Although, commercialized standard piezoelectric transducers are available, they can not fulfill the specific requirements such as the radiation surface contour and the vibration amplitude distribution. Therefore the transducers must be specially designed for the bearing system.

Previously reported designs of squeeze film levitation bearings often used bending piezoelectric elements as the active part to generate the levitation effect. Such designs are rather compact, but the vibration is very sensitive to the load. At high-load situation, the vibration amplitude is "pressed" down, which leads to a dramatic reduction of levitation force. To avoid such problems, for the present application, a half wavelength Langevin type piezoelectric transducer (as shown in Fig. 5.8) is selected as the vibration source. Langevin type transducers are known to be very stable when subjected to load and have many distinct advantages as already discussed in Sec. 5.2.

For the present application, the desired working frequency of the transducer is 20 kHz at the first longitudinal vibration mode. The expected unloaded vibration amplitude at the radiation surface is 15 μm in normal operation state. The maximum allowed output power of the transducer is designed to be 1000 W. The piezoelectric ceramic rings used in this investigation are provided by PI Ceramic GmbH. in Germany, namely PIC-181. PIC-181 is a modified lead zirconate - lead titanate material with an extremely high mechanical quality factor and a high Curie temperature. This material is destined for the use in high-power acoustic applications. Furthermore, the good temperature and time stability of its dielectric and elasticity constants makes it suitable for resonance-mode ultrasonic applications. The specification is listed in Table 9.1 (25).

In this application, a relatively large radiation surface (about 8 cm^2) and high vibration amplitude (up to 15 μm) are required. It requires very high input power to achieve the required amplitude directly from the deformation of the ceramic rings

| Parameter	Symbol	Value	Unit
Density	ρ	7800	kg/m^3
Electromechanical coupling factor	k_{33}	0.66	
Piezoelectric charge constant	d_{33}	265	10^{-12} C/N
Piezoelectric voltage constant	g_{33}	25	10^{-3} Vm/N
Elastic constant	C_{33}^D	16.6	10^{10} N/m^2
Mechanical quality factor	Q_m	2000	
Static compressive strength		600	MPa

Table 9.1: Specifications of PIC-181

without amplification. Therefore a horn shape transducer has been designed to amplify the vibration amplitude. For a certain area of radiation surface, a larger cross-section area of the piezoelectric ceramic ring will result in a larger amplification factor. Thus, ceramic rings of 50 mm in outer diameter, 20 mm in inner diameter and 5 mm in thickness are selected.

The required volume of the ceramic rings can be estimated from the expected maximum output power. For PIC-181, the power capacity is commonly said to range from 1.5 to 3 W/cm^{3}kHz for high power applications (1). Considering the selected ceramic rings, the volume of one ring is 8.3cm^3. At the designed working frequency of 20kHz, each ring can provide about 250 W to 500 W output power. Thus, in order to fulfill the designed output power, four ceramics rings are mounted in each transducer. Of course, higher power can be achieved by adding more ceramic rings in the transducer. It will also result in higher vibration amplitude without increasing input power. However the amount of the ceramic rings is limited by the structure of the transducer, and furthermore, the transducer will become more sensitive to the load with more ceramic rings (42).

The material selected for the front and back covers are Titanium alloy and stainless steel. The selected combination provides the best balance of acoustic impedance matching and mechanical strength.
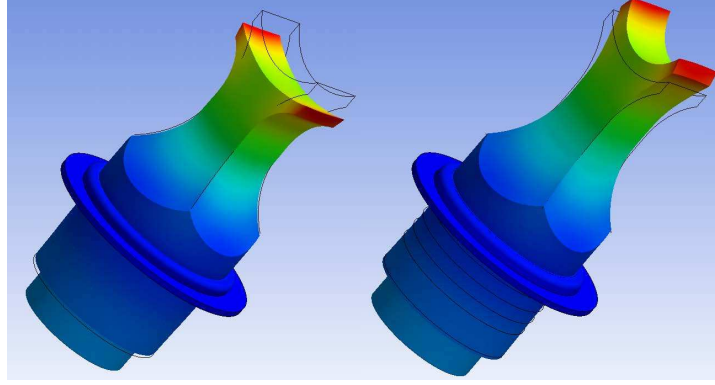
Figure 9.2: FEM simulation result of the ultrasonic transducer

At first, the dimension of the transducer is calculated as the example given in Sec. 5.2.2 with nodal plane located in the front cover. Lengths of each part are calculated according to Equ. 5.9 and 5.10. A FEM model is built according to the obtained dimensions by employing ANSYS software, since the Finite Element Method (FEM) can give a reliable indication of the natural frequency and the vibration mode. By repeating the modal analysis and modifying the dimensional parameters, the transducer is tuned to match the designed natural frequency and vibration mode. A concave radiation surface to match the spindle surface is also modified on the front cover. The FEM simulation result of the transducer is shown in Fig. 9.2.

The transducers are manufactured according to the dimensions from FEM optimization. After assembling, the frequency response of all three transducers was measured using an impedance analyzer. The admittance and phase versus frequency diagram of all three transducers are shown in Fig. 9.3. The result shows that the resonant and anti-resonant frequencies at the desired vibration mode are close to 20 kHz and 20.8 kHz respectively. Despite slight differences among the three transducers, the measurements match with the simulation results quite well. Under unloaded condition, the vibration amplitude at the middle of the radiation surface is measured as 12 μm using a laser interferometer when the input power is approximately 50 Watt.
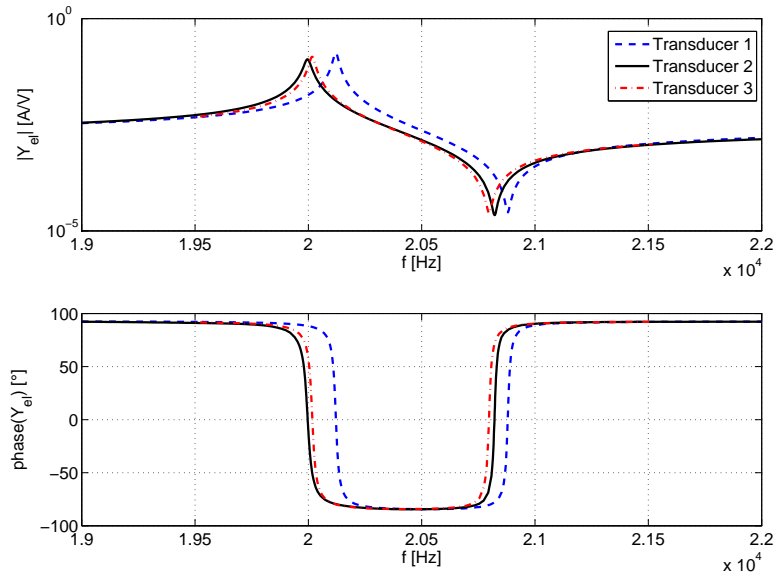
Figure 9.3: Measured frequency response of the ultrasonic transducers
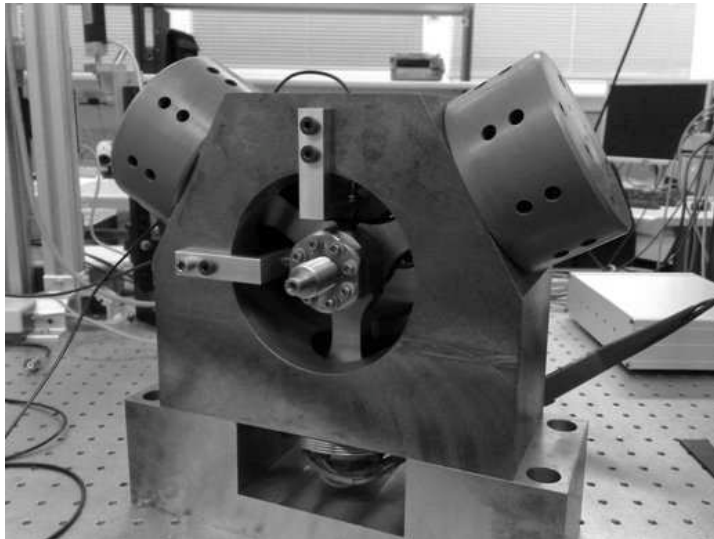
Figure 9.4: Prototype of the proposed squeeze film bearing

9.1.2 The spindle-bearing system

A spindle-bearing system is constructed in the lab to investigate the behavior of the presented squeeze film journal bearing. The realized prototype system is shown in Fig. 9.4. The system consists of a spindle supported by the presented bearing at one end and a ball bearing at the other end. The distance between the two bearings is 150 mm. Two eddy current displacement sensors are installed to measure the spindle position. The diameter of the spindle is 49.94 mm which forms a mean bearing clearance of 30 μm with the bearing journal. Each transducer is driven in its resonant frequency. After manually adjusting the input power of each transducer, the bearing system provides steady, friction-free suspension to the spindle.

9.2 Testing the prototype bearing

The levitation forces at different gap distances in vertical direction are measured using the eddy current sensor and a load cell. External load is applied on the spindle in the gravity direction through the load cell. The maximum load is measured right before contact happens between the bearing and the spindle. The results are plotted in Fig. 9.5 together with the calculated results from the presented mathematical models by utilizing the actual parameter values. Constant vibration amplitude of 20 μm of the transducer is maintained during the measurement. The measurement results agree very well with the numerical results of Reynolds equation. A load-carrying force of 51 N (6.37 N/cm^2)is obtained when the gap distance is 28 μm at the bottom transducer. Seeing the trend in Fig. 9.5, higher bearing force may be achieved by further reducing the gap distance. But this is limited by the manufacturing accuracy of the bearing surfaces. Some region starts to get in contact by further reduction of the gap.

The run-out error of the levitated spindle is measured when the spindle is stationary at the beginning and starts rotating after some time. The results are shown in Fig. 9.6. It can be seen that the levitation is very stable when the spindle is stationary. When the spindle is rotating, periodic error of a few micrometers is measured which is subjected to the form error and surface roughness of the spindle. The run-out error of the center of the spindle remains very small.
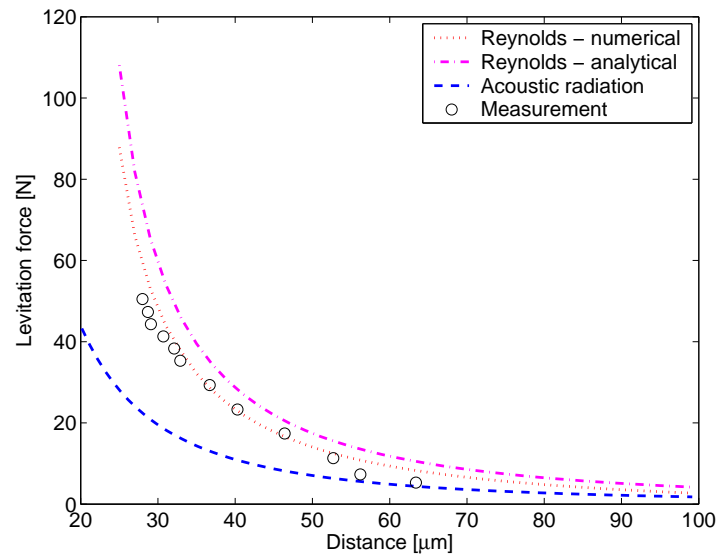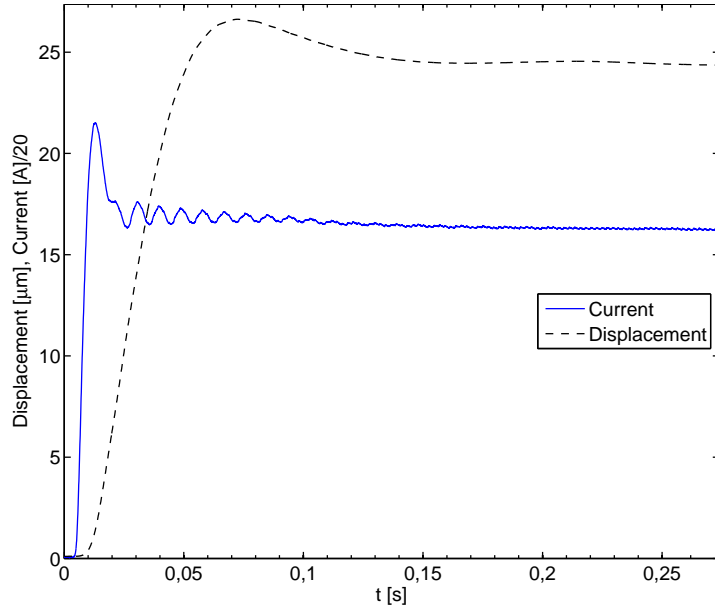
Figure 9.5: Load capacity versus levitation distance at constant vibration amplitude of 20 micrometers
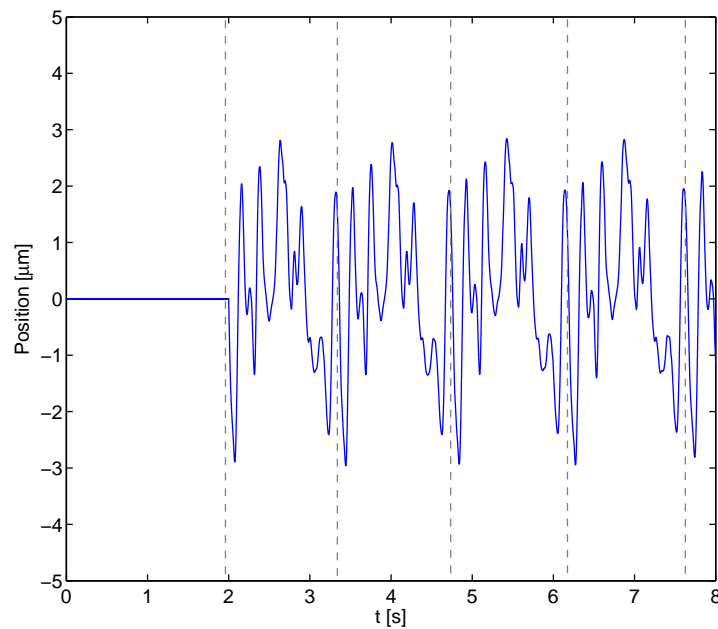
Figure 9.6: Spindle run-out error during levitation

Figure 9.7: Displacement response of the spindle center subjected to a current step

The load-carrying force of the proposed bearing is the average force from every compress-release cycle between the bearing and the spindle. For driving frequency of 20 kHz, the time that is needed for one compress-release cycle is 50 μs. When the spindle is rotating, a lateral movement is generated between the bearing and the spindle surfaces. The lateral movement has the line speed of the rotating spindle. For a relatively high rotation speed of 10000 rpm, the line speed of spindle (50 mm diameter) is 8.33 m/s. The spindle rotates 3 degree in one compress-release cycle, and the relative lateral movement between two surfaces is 0.42 mm, which is much smaller compared to the circumference of the bearing. Therefore, the spindle can be considered as staying still within one compress-release cycle. We can conclude that the levitation force is not sensitive to the rotation speed. The proposed bearing is suitable for both low and high speed applications.

Figure 9.7 shows the displacement response of the levitated spindle subjected to a current amplitude envelope step. The current amplitude is proportional to the vibration velocity amplitude V_0, which is in turn proportional to the levitation force according to Equ. 8.11. Thus figure 9.7 is the step response of a mass-spring-damper system excited by a force. This step response can be used in the design of a PID controller with a classic method like "open loop method" (24) to determine the optimal parameter of

97

the controller.

9.3 Conclusion

In this chapter, a squeeze film bearing has been developed which can provide a non-contact support to rotating parts. The proposed bearing does not require external pressurized air or liquid supply. The bearing is naturally stable since the squeeze film levitation force is a repelling force, which increases as the distance is getting smaller. The spindle is "pushed" from all around and held at the equilibrium position. A solid steel spindle with diameter of 50 mm has been successfully levitated. The maximum load capacity of 51 N is achieved at the vibration amplitude of 20 μm. This is considerably larger than that of all other squeeze film bearing presented before (17; 51; 65; 66) whose load capacities are usually within a few Newton. Load capacity can be further increased by increasing the vibration amplitude and by improving the surface quality. The proposed bearing can be applied to support heavy rotors such as spindles in machine tools.

10

Summary and outlook

Ultrasonic levitation has been investigated theoretically and experimentally to construct non-contact bearing systems. Both type of ultrasonic levitation, standing wave and squeeze film type, are studied with two prototype systems.

For standing wave type ultrasonic levitation, a one dimensional acoustic levitation system using ultrasonic standing wave is proposed with detailed theoretical analysis. The proposed system is able to levitate large planar object (much larger than the sound wavelength) at a position of multiple times of a half wavelength of the sound wave (much higher than squeeze film levitation system). The proposed levitation system is suitable for building non-contact bearings for applications which require low load capacity but very high separation distance. The theoretical model for the proposed levitation system is established. A prototype system is constructed accordingly. A CD is successfully levitated with the proposed system at a height of half a wavelength. The levitation forces at different distances are measured. A force of about 1 N is observed at the position of half wavelength in front of the sound radiator.

Squeeze film type ultrasonic levitation has been investigated theoretically to improve the achievable levitation capacity. Excursion ratio ϵ and squeeze number σ are found to be the most crucial parameters that determine the levitation capacity. A good surface finishing and form accuracy are also important for a squeeze film levitation system to achieve higher levitation capacity. A higher vibration amplitude is helpful to achieve higher levitation capacity when the mean gap δ can not be further reduced. The

theoretical model is validated using experimental results. A novel non-contact journal bearing is presented based on the theoretical investigation, which aims on high load capacity. The proposed bearing is actuated by Langevin type piezoelectric transducers. A solid steel spindle with diameter of 50 mm has been successfully levitated. The maximum load capacity of 51 N (6.37 N/cm^2) is achieved at the vibration amplitude of 20 μm. This is considerably larger than the previously reported squeeze film bearings (17; 51; 65; 66) whose load capacities are usually within a few Newton (less than 1 N/cm^2). The achieved load capacity from the proposed bearing is already comparable to a conventional air bearing of similar size, whose load capacity is usually between 10 to 20 N/cm^2. The proposed bearing has very stable performance in both low and high rotation speed.

At high rotational speed, an aerodynamic pressure can be generated in the air gap. This aerodynamic pressure can give additional load capacity to the bearing system. The influence on the squeeze film pressure caused by the lateral relative motion between the spindle and the bearing surface during rotation should be studied in the future. The presented bearing shows good dynamic behaviors. By implementing a feedback control system, an active bearing with run-out error and external disturbance compensation can be achieved.

Bibliography

[1] A. Abdullah, M. Shahini , and A. Pak. An approach to design a high power piezoelectric ultrasonic transducer. *Journal of Electroceramics*, 2008. 43, 92

[2] O.V. Abramov. *High-intensity ultrasonics: theory and industrial applications*. Gordon and Breach Science Publishers, 1998. 27

[3] T. Amano, Y. Koike, K. Nakamura, S. Ueha, and Y. Hashimoto. A Multi-Transducer Near Field Acoustic Levitation System for Noncontact Transportation of Large-Sized Planar Objects. *Japanese Journal of Applied Physics*, 39:2982, May 2000. 15

[4] M. Barmatz and P. Collas. Acoustic radiation potential on a sphere in plane, cylindrical, and spherical standing wave fields. *Acoustical Society of America Journal*, 77:928–945, March 1985. 8

[5] H. E. Bass, L. C. Sutherland, and A. J. Zuckerwar. Atmospheric absorption of sound: Update. *The Journal of the Acoustical Society of America*, 88(4):2019–2021, 1990. 30, 31, 60

[6] H. E. Bass, L. C. Sutherland, A. J. Zuckerwar, D. T. Blackstock, and D. M. Hester. Atmospheric absorption of sound: Further developments. *Acoustical Society of America Journal*, 97(1):680–683, 1995. 30, 60

[7] Robert . D. Blevins. *Formulas for Natural Frequency and Mode Shape*. Malabar, Florida: Krieger Publishing., 2001. 53, 54

[8] K. Bücks and H. Müller. Über einige Beobachtungen an schwingenden Piezo-quarzen und ihrem Schallfeld. *Z. Phys.*, 84:75–86, 1933. 10

BIBLIOGRAPHY

[9] B.-T. Chu and R. E. Apfel. Acoustic radiation pressure produced by a beam sound. *Acoustical Society of America Journal*, 72:1673–1687, December 1982. 32

[10] B.-T. Chu and R. E. Apfel. Response to the Comments of Nyborg and Rooney [J. Acoust. Soc. Am. 75, 263-264 (1984)] . *Acoustical Society of America Journal*, 75:1003–1004, March 1984. 13

[11] N. Daidzic. *Nonlinear droplet oscillations and evaporation in an ultrasonic levitator*. PhD thesis, Lehrstuhl fuer Stroemungsmechanik, Friedrich-Alexander-Universitaet Erlangen, 1995. 7

[12] T. F. W. Embleton. Mean Force on a Sphere in a Spherical Sound Field. I. (Theoretical). *Acoustical Society of America Journal*, 26:40, 1954. 8

[13] Claude L. Emmerich. Piezoelectric oscillating bearing. *US patent No. 3351393*, (3351393), November 1967. 16

[14] Teitelbaum Bernard R. Farron, John R. Squeeze film bearings. *US patent No. 3471205*, (3471205), October 1969. 16, 89

[15] B. Fu. *Piezoelectric Actuator Design via Multiobjective Optimization Methods*. PhD thesis, Heinz Nixdorf Institute, University of Paderborn, 2005. 41, 46

[16] L. P. Gor'kov. On the Forces Acting on a Small Particle in an Acoustical Field in an Ideal Fluid. *Soviet Physics Doklady*, 6:773, March 1962. 8

[17] D.N. Ha, T.A. Stolarski , and S. Yoshimoto. An aerodynamic bearing with adjustable geometry and self-lifting capacity. part 1: self-lift capacity by squeeze film. *Proceedings of the I MECH E Part J Journal of Engineering Tribology*, 219:33–39(7), January 2005. 20, 98, 100

[18] B. J. Hamrock. *Fundamentals of Fluid Film Lubrication*. McGraw-Hill Companies, 1994. 13, 14, 76, 77

[19] T. Hasegawa. Acoustic-Radiation Force on a Solid Elastic Sphere. *Acoustical Society of America Journal*, 46:1139, 1969. 7

[20] Y. Hashimoto. Transporting objects without contact using flexural travelling waves. *Acoustical Society of America Journal*, 103:3230–3233, 1998. 15

[21] Y. Hashimoto, Y. Koike, and S. Ueha. Near-field acoustic levitation of planar specimens using flexural vibration. *Acoustical Society of America Journal*, 100:2057–2061, October 1996. 13, 21

[22] T. Hemsel. *Untersuchung und Weiterentwicklung linearer piezoelecktrischer Schwingungsantriebe.* PhD thesis, Heinz Nixdorf Institut, Universität Paderborn, 2001. 39, 40, 41

[23] J. Höppner. *Verfahren zur berhrungslosen handhabung mittels leistungsstarker schallwandler (in German).* PhD thesis, Technische Universität München, 2002. 57, 77

[24] M. Horn and N. Dourdoumans. *Regelungstechnik (Control systems).* PEARSON Studium, 2004. 97

[25] http://www.piceramic.de/. 91

[26] T. Ide, J. R. Friend, K. Nakamura, and S. Ueha. A Low-Profile Design for the Noncontact Ultrasonically Levitated Stage. *Japanese Journal of Applied Physics*, 44:4662, June 2005. 17, 18

[27] T. Ikeda. *Fundamentals of Piezoelectricity.* Oxford University Press, 1996. 36

[28] L.V. King. On the acoustic radiation pressure on spheres. *Proc. R. Soc. London Ser.*, 1934. 7, 9, 10

[29] D. Koyama, T. Ide, and J.R. Friend. An ultrasonically levitated non-contact sliding table with the traveling vibrations on fine-ceramic beams. In *IEEE Ultrasonics Symposium*, pages 1838–1541, 2005. 18, 19

[30] C. P. Lee and T. G. Wang. Acoustic radiation pressure . *Acoustical Society of America Journal*, 94:1099–1109, August 1993. 32, 33, 55, 57, 74

[31] E.G. Lierke. Acoustic levitation a comprehensive survey of principles and applications. *Acta Acustica united with Acustica*, 82, March 1996. 8

[32] L.G. Lierke, R. Grossbach, and P. Clancy. Acoustic positioning for space processing of materials science samples in mirror furnaces. In *1983 IEEE Ultrasonic Symposium Proceedings*, page 1129, 1983. 10

[33] W. Littmann. *Piezoelektrische, resonant betriebene Ultraschall-Leistungswandler mit nichtlinearen mechanischen Randbedingungen (in German).* PhD thesis, University of Paderborn, Heinz Nixdorf Institute, 2003. 37, 42, 64

[34] W. Littmann, T. Hemsel, C. Kauczor, J. Wallaschek, and M. Sinha. Load-adaptive phase-controller for resonant driven piezoelectric devices. In *World Congress Ultrasonics*, Paris, Sep. 2003. 48, 64

[35] D. Y. Ma and H. Shen. *Handbook of Acoustics.* Science Press, 2006. 56

[36] W.A. Michael. , A gas film lubrication study part II: numerical solution of the Reynolds equation for finite slider bearings. *IBM Journal*, pages 286–259, 1959. 13, 14

[37] A. Minikes and I. Bucher. Comparing numerical and analytical solutions for squeeze-film levitation force. *Journal of Fluids and Structures*, 22:713–719, July 2006. 14, 77

[38] A. Minikes, I. Bucher, and S. Haber. Levitation force induced by pressure radiation in gas squeeze films. *Acoustical Society of America Journal*, 116:217–226, July 2004. 14, 77

[39] H. Nomura, T. Kamakura, and K. Matsuda. Theoretical and experimental examination of near-field acoustic levitation. *Acoustical Society of America Journal*, 111:1578–1583, April 2002. 14, 77

[40] T. Otsuka, K. Higuchi, and K. Seya. Ultrasonic levitation by stepped circular vibrating plate. In *The 10th Symposium on Ultrasonic Electronics*, page 170, 1989. 10

[41] J. H. Poynting and J. J. Thomson. *A Textbook of Physics.* Charles Griffin & Co., 1904. 7

[42] M. Prokic. *Piezoelectric Transducers Modeling and Characterization.* M.P. Interconsulting, 2004. 92

[43] M. D. Radmanovic and D. D. Mancic. *Design and Modelling of Power Ultrasonic Transducers.* M.P. Interconsulting, 2004. 43

[44] L. Rayleigh. On the pressure of vibrations. *Philosophical magazine*, 3:338, 1902. 31

[45] R. Reinhart, J. Höppner, and J. Zimmermann. Non-contact wafer handling using high-intensity ultrasonics. In *IEEE/SEMI Advanced Semiconductor Manufacturing Conference*, pages 139–140, 2001. 51

[46] T. D. Rossing. *Springer Handbook of Acoustics*. Springer New York, 2007. 27, 30, 32, 56

[47] E.O.J. Salbu. Compressible squeeze films and squeeze bearings. *Journal of Basic Engineering*, 86:355–366, 1964. 11, 16, 77, 78, 79, 86

[48] NY) Scranton, Robert A. (South Salem. Planar and cylindrical oscillating pneumatodynamic bearings. *US patent No. 4666315*, (4666315), May 1987. 16

[49] C. H. Sherman and J. L. Butler. *Transducers and Arrays for Underwater Sound*. Springer Publishing Company, Incorporated, 2007. 43, 54, 55

[50] L. J. Smith. Use of phase-locked-loop control for driving ultrasonic transducers. *NATIONAL AERONAUTICS AND SPACE ADMINISTRATION*, August 1966. 48

[51] T A Stolarski. Performance of a self-lifting linear air contact. *Proceedings of the I MECH E Part C Journal of Mechanical Engineering Science*, 221:1103–1115(13), 2007. 18, 19, 20, 77, 89, 98, 100

[52] E. H. Trinh. Compact acoustic levitation device for studies in fluid dynamics and material science in the laboratory and microgravity. *Review of Scientific Instruments*, 56:2059–2065, November 1985. 10

[53] V. Vandaele, P. Lambert, and A. Delchambre. Non-contact handling in microassembly: Acoustical levitation. *Precision Engineering*, 29:491–505, 2005. 7, 8

[54] J. Wallaschek. Systementwurf piezoelektrischer Aktoren. *VDI Bildungswerk Mechatronik Workshop*, 2000. 37, 38

[55] T.G. Wang and M.M. Saffren. Acoustic chamber for weightless positioning. *AIAA paper*, 155, 1974. 10

[56] Lyle F. Warnock Jr. Dynamic gas film supported inertial instrument. *US patent No. 3339421*, (3339421), September 1967. 16, 89

[57] P. J. Westervelt. The mean pressure and velocity in a plane acoustic wave in a gas. *Acoustical Society of America Journal*, 22:319–327, 1950. 8

[58] P. J. Westervelt. The Theory of Steady Forces Caused by Sound Waves. *Acoustical Society of America Journal*, 23:312–315, 1951. 8

[59] P. J. Westervelt. Acoustic radiation pressure. *Acoustical Society of America Journal*, 29:26–29, 1957. 8

[60] R.R. Whymark. Acoustic field positioning for containerless processing. *Ultrasonics*, 13:251–261, November 1975. 10, 11

[61] M. Wiesendanger. *Squeeze film air bearings using piezoelectric bending elements.* PhD thesis, Ecole polytechnique federale de Lausanne, 2001. 12, 13, 14, 17, 18, 47, 77, 89

[62] W. J. Xie, C. D. Cao, Y. J. Lü, Z. Y. Hong, and B. Wei. Acoustic method for levitation of small living animals. *Applied Physics Letters*, 89(21):214102, November 2006. 11

[63] W. J. Xie and B. Wei. Parametric study of single-axis acoustic levitation. *Applied Physics Letters*, 79:881, August 2001. 10

[64] W. J. Xie and B. Wei. Dynamics of acoustically levitated disk samples. *Physical Review*, 70(4):046611, October 2004. 8

[65] S. Yoshimoto, Y. Anno, and K. Hamanaka. Float characteristics of squeeze-film gas bearing with elastic hinges for linear motion guide. *JSME international journal*, 1997. 18, 20, 98, 100

[66] S. Yoshimoto, H. Kobayashi , and M. Miyatake. Float characteristics of a squeeze-film air bearing for a linear motion guide using ultrasonic vibration. *Tribology Inter.*, 40:503–511, 2007. 20, 21, 89, 98, 100

[67] L. Zipser and S. Lindner. Visualisation of vortexes and acoustic sound waves. In *Proceedings of 17th Int. Congress on Acoustics*, volume I, Physical Acoustics part B, Ultrasonics, quantum acoustics and physical effect of sound, pages 24–25, 2001. 68

[68] L. Zipser, S. Lindner, and R. Behrendt. Anordnung zur Messung und visuellen Darstellung von Schalldruckfeldern (Equipment for measurement and visualization of sound fields). *Patent DE 10 057 922*, 2000. 68